Theses and Dissertations   Student Graduate Works

3-2020

Comparison of the Accuracy of Rayleigh-Rice Polarization Factors to Improve Microfacet BRDF Models

Rachel L. Wolfgang

COMPARISON OF THE ACCURACY OF
RAYLEIGH-RICE POLARIZATION FACTORS
TO IMPROVE MICROFACET BRDF
MODELS

THESIS

Rachel L. Wolfgang, Second Lieutenant, USAF

AFIT-ENP-MS-20-M-123

DEPARTMENT OF THE AIR FORCE
AIR UNIVERSITY

AIR FORCE INSTITUTE OF TECHNOLOGY

Wright-Patterson Air Force Base, Ohio

The views expressed in this thesis are those of the author and do not reflect the official policy or position of the United States Air Force, Department of Defense, or the United States Government. This material is declared a work of the U.S. Government and is not subject to copyright protection in the United States.

AFIT-ENP-MS-20-M-123

COMPARISON OF THE ACCURACY OF RAYLEIGH-RICE POLARIZATION FACTORS TO IMPROVE MICROFACET BRDF MODELS

THESIS

Presented to the Faculty

Department of Engineering Physics

Graduate School of Engineering and Management

Air Force Institute of Technology

Air University

Air Education and Training Command

in Partial Fulfillment of the Requirements for the

Degree of Master of Science in Applied Physics

Rachel L. Wolfgang, B.S.

Second Lieutenant, USAF

26 March 2020

DISTRIBUTION STATEMENT A
APPROVED FOR PUBLIC RELEASE; DISTRIBUTION UNLIMITED.

COMPARISON OF THE ACCURACY OF RAYLEIGH-RICE POLARIZATION
FACTORS TO IMPROVE MICROFACET BRDF MODELS

Rachel L. Wolfgang, B.S.
Second Lieutenant, USAF

Committee Membership:

Lt Col Samuel D. Butler, Ph.D.
Chairman

Michael A. Marciniak, Ph.D.
Member

Abstract

The bidirectional reflectance distribution function (BRDF) quantifies how light interacts and reflects off of materials directionally. Microfacet BRDF models, which are more computationally simple than wave optics models, assume that a surface has many small microfacets making up the roughness of the surface. Despite their computational simplicity in applications in remote sensing and scene generation, microfacet models lack the physical accuracy of wave optics models. In a previous work, Butler proposed to replace the Fresnel reflectance term of microfacet models with the Rayleigh-Rice polarization factor, Q, to create a more accurate model. Problems with the geometric attenuation term in microfacet models extended the approximation to replace the Fresnel terms with Q. Ewing found this modification to be effective for 12 of 18 materials when used with a Hyper-Cauchy distribution function, but polarization data was not considered. This work examines the novel model that combines microfacet and wave optics terms for its accuracy in the pp and ss polarized cases individually. The model is fitted to the polarized data in each case, using the polarization factor Q, and the resulting fitted parameters are used to investigate whether parameters obtained using the ss and pp polarization may be used on the oppositely polarized or unpolarized data. General parameters are also determined for each material and compared. Fitting parameters are found to be unreliable for ss polarization, especially for the index of refraction. Parameters fitted from pp polarization data fit cross-term data better than those from ss polarization data for at least nine of the fourteen materials, indicating that more research must be done to make Q in the ss case more accurate. Because they are more accurate, general fitting parameters for pp polarization have potential to be used in detecting material properties. Model trends

are determined to guide future work in refining polarimetric models.

Acknowledgements

I would like to thank Joe Constantino of the Air Force Research Lab, Materials and Manufacturing Directorate, Optical Measurements Facility (OMF) for collecting and providing the data used in this work.

Thank you to my classmates, friends, and family for their support throughout the trials and tribulations of graduate school.

I would also like to thank my advisor, Lt Col Butler for guiding me on the thesis journey and answering any question I had, no matter how trivial.

Rachel L. Wolfgang

Table of Contents

List of Figures

xi

List of Tables

xiv

COMPARISON OF THE ACCURACY OF RAYLEIGH-RICE POLARIZATION
FACTORS TO IMPROVE MICROFACET BRDF MODELS

I. Introduction

1.1 Motivation and Background

The Air Force conducts many missions emphasizing a multi-dimensional battlespace and highlighting the interoperability of capabilities. Remote sensing is an important aspect used in both of these situations in order to receive information to make decisions. Detection and identification of entities, both compliant and non-compliant is important to improve stealth operations or be aware of adverse assets.

As detectors, both visible and infrared (IR) become more sophisticated, emissions and reflections from aircraft systems may be more conspicuous than desired. Aircraft surface coatings, or paints contribute largely to an aircraft's signature in the electromagnetic spectrum, based on the emissive-reflective quality of the paint. The magnitude of these paint emissions and reflections can be quantitatively determined using an optical scatter distribution of the paint [1]. Not only are reflections and emissions of aircraft paint important, but the bidirectional reflectance can be useful in scene generation and remote sensing, as simplified reflection and refraction laws are only accurate for mirrors or perfectly diffuse scatterers, not in general [2]. The bidirectional reflectance distribution function (BRDF) describes how light interacts with realistic surfaces. Although many BRDF models exist, a computationally simple geometric-optics-based class of models uses microfacet theory. From a previous work comparing the microfacet and diffraction theory BRDF models, an approximation

1

was found between polarization terms [3]. Namely, the Fresnel reflectance typically used in microfacet models and the Rayleigh-Rice polarization factor used in diffraction theory models were compared and found that the model using this approximation was more physically accurate. While this approximation from the previous work is more physically accurate, only unpolarized versions were considered.

Since BRDF models are not predictive – they rely on fitting to collected data on individual materials to be considered accurate – investigation into how these polarimetric terms work is necessary. Specifically, fitting a BRDF model to polarized data for this approximated polarization factor will allow more accurate BRDF models when it comes to fitting polarized data.

1.2   Research Objective

A novel BRDF model that modifies the cross section conversion and geometric attenuation terms of microfacet BRDF models with the new polarization factor from a previous work will be investigated for different polarization states [4]. This model's variables will be fitted for each polarization state against the raw data of a variety of paints, both diffuse and specular. The resulting model parameters from the fit of one polarization will then be tested against the other polarization to determine if these parameters are material-specific, or how different they are from each other.

Polarization in BRDF models has had various forms from using Jones and Mueller matrices and other polarimetric terms. This novel investigation into combining the simplicity of the microfacet BRDF and the physical accuracy of the modified polarization term will allow further investigation into making an all-encompassing BRDF model that can be accurate for both unpolarized and polarized light.

For materials measured between LWIR to UV, the polarization fitting parameters are presented and compared to investigate if there are differences between one polar-

2

ization case to another. In addition, the interchangeability of the fitted parameters is tested for each material. Fitted parameters from fitting to ss polarization data will be put into the model for pp polarization data (and vice versa) to determine whether there is a trend, if the parameters can be used universally for a material, or if more work needs to be done in making this approximation more accurate for polarization data.

As a summary of the results, parameters that optimized the fits of the model at each incident angle and that were found from fitting all of the data for a material were found and compared. For a common incident angle to all materials, both sets of parameters found that pp parameters better modeled pp data, and modeled ss and unpolarized data better than when compared to when ss parameters tried to do the same. This was the case for the majority of materials. In addition, ss parameters were found to be unreliable because of how often the upper and lower bounds for the fit were outputted. While a conlusion was made that more work needs to be done on the ss Rayleigh-Rice factor, this work also finds that the parameters for 'all' incident angles of each material in pp polarization may be used in remote sensing to determine the index of refraction, or information that could identify a material.

1.3 Document Structure

This thesis will start with background information in Chapter II. The microfacet BRDF model will be defined, along with the novel polarization term used. Chapter III will discuss the types of materials used in this analysis and the process used to determine the fitted parameters will be presented in this chapter. Chapter IV presents the results of the fitted model to the polarization states for each material, with an analysis on how the fitted model parameters compare between polarization and materials. Finally Chapter V will include summarize the conclusions, and offer

3

recommendations for future work, including looking into additional polarization states and microfacet polarimetric BRDF models.

II. Background

2.1 Electromagnetics

Maxwell's equations describe the classical electromagnetic field, though they are mathematical abstractions based on experimental results. Assuming linear media, The equations in SI units are [5]

$$\nabla \cdot \tilde{\mathbf{E}} = \frac{\rho}{\epsilon} \tag{1}$$

$$\nabla \cdot \tilde{\mathbf{B}} = 0 \tag{2}$$

$$\nabla \times \tilde{\mathbf{E}} + \frac{\partial B}{\partial t} = 0 \tag{3}$$

$$\nabla \times \tilde{\mathbf{B}} - \epsilon\mu\frac{\partial E}{\partial t} = \mu\tilde{\mathbf{J}} \tag{4}$$

where $\vec{E}$ and $\vec{B}$ are electric and magnetic fields, $\vec{J}$ is current density, ρ is charge density, ϵ is permittivity, and μ is permeability. In free space, these equations simplify as $\vec{J} = 0$, $\rho = 0$, $\epsilon = \epsilon_0$, and $\mu = \mu_0$.

For waves incident on a surface, the law of reflection, $\theta_i = \theta_s$, expresses that the angle of incidence equals the angle of reflection. Snell's law describes expresses the angle of the refracted wave as [5]

$$\tilde{n}_i \sin\theta_i = \tilde{n}_s \sin\theta_s \tag{5}$$

where $\tilde{n}_i$ and $\tilde{n}_s$ are the incident and scattered indices of refraction of the media, respectively. The index of refraction is defined as [5]

$$\tilde{n} = n + i\kappa \tag{6}$$

5

where the n is the real part of the index of refraction of the material, which describes how fast light passes through a material, and κ is the imaginary part of the material's index of refraction, which indicates the amount of attenuation of the wave through the material. Both of these will be used in Chapter III as fitting parameters for the BRDF models when fitting to the BRDF experimental data.

Fresnel reflectance, F is commonly used in microfacet models for s and p polarizations given by [5] and used in the form from [6]

$$r_s = \frac{\tilde{n}_1 \cos(\theta_d) - \tilde{n}_2 \sqrt{1 - \left| \frac{\tilde{n}_1}{\tilde{n}_2} \sin(\theta_d) \right|^2}}{\tilde{n}_1 \cos(\theta_d) + \tilde{n}_2 \sqrt{1 - \left| \frac{\tilde{n}_1}{\tilde{n}_2} \sin(\theta_d) \right|^2}}, \tag{7}$$

$$r_p = \frac{\tilde{n}_1 \sqrt{1 - \left| \frac{\tilde{n}_1}{\tilde{n}_2} \sin(\theta_d) \right|^2} - \tilde{n}_2 \cos(\theta_d)}{\tilde{n}_1 \sqrt{1 - \left| \frac{\tilde{n}_1}{\tilde{n}_2} \sin(\theta_d) \right|^2} + \tilde{n}_2 \cos(\theta_d)}, \tag{8}$$

where r_s is the component of the electric field perpendicular to the plane of incidence and r_p is the component of the electric field parallel to the plane of incidence.

In this work, $\tilde{n}_1$, is approximated to be 1, meaning that the incident light is from air ($\tilde{n} = 1.0003 \approx 1$), while $\tilde{n}_2$ is left as a fitting parameter for various materials, given their raw BRDF data. The square of these equations is the intensity of the reflected light in the s and p polarization, respectively. The Fresnel equation for unpolarized light is

$$F(\theta_d) = \frac{|r_p|^2 + |r_s|^2}{2}. \tag{9}$$

6

2.2 BRDF

The BRDF provides a way to quantify how light interacts and reflects off of materials. Formally, the BRDF was defined by Nicodemus [7]

$$f_r(\theta_i, \phi_i, \theta_s, \phi_s, \lambda) = \frac{dL_r(\theta_i, \phi_i, \theta_s, \phi_s, \lambda)}{dE_i(\theta_i, \phi_i, \lambda)} \tag{10}$$

where the reflected radiance, dL_r is a function of the spherical coordinates θ and ϕ for the incident (i) and scattered (s) light and wavelength (λ), and the incident irradiance, dE_i is a function of the angles of the incident light and wavelength. Often, the wavelength dependence is neglected in many BRDF models. Physics-based BRDF models are divided into two classes: microfacet models and wave-optics (diffraction theory) models. Typically, diffraction theory models are more physically accurate but at the price of being significantly more computationally complex. These models are based on first-principles optical physics and an electromagnetic wave solution requires large computational capability and is not practical for most BRDF applications of interest to the Air Force, such as remote sensing or near-realtime scene generation. Microfacet models, on the other hand, are simpler but are less physically accurate.

There are two extreme cases where materials are easy to model, which are Lambertian and specular. A perfectly diffuse, or Lambertian surface is represented as

$$f_r = \frac{\rho}{\pi} \tag{11}$$

where ρ is the surface's overall (unitless) reflectance and π represents the plane wave reflecting evenly for all incident and reflected angles over a hemisphere. Specular reflectance on the other hand, is represented as

$$f_r(\theta_i, \theta_s, \phi_s) = \rho\delta(\theta_i - \theta_s)\delta(\phi_s - \pi). \tag{12}$$

7

This equation obeys Snell's law and has a BRDF value of 0 every except at $\theta_s = \theta_i$ and $\phi_s = \phi_i \pm \pi$. In this work, the assumption $\phi_i = 0$ is made to neglect out of plane scatter. Real surface reflections are a combination of both specular and Lambertian reflections. Reflections off real materials have a specular reflection direction where the BRDF is larger than at other angles.

2.3 Microfacet BRDF

BRDF in a microfacet model is often calculated as the sum of the specular, volumetric, and diffuse terms in a simplified form by Butler [8]

$$f_r(\theta_i, \theta_s) = \rho_s \cdot G(\theta_i, \theta_s) \cdot D(\theta_h) \cdot F(\theta_d) \cdot \sigma(\theta_i, \theta_s) + \rho_v \cdot V(\theta_i, \theta_s) + \frac{\rho_d}{\pi} \tag{13}$$

where ρ_s, ρ_v, and ρ_d are the specular, volumetric and diffuse fitting parameters, $G(\theta_i, \theta_s)$ is the geometric attenuation term, $D(\theta_h)$ is the microfacet distribution function which is dependent on the half-angle, θ_h, $F(\theta_d)$ is the Fresnel reflectance for unpolarized light as a function of the difference vector, θ_d, and σ is the cross-section conversion term. The half-angle and difference vector, called Rusinkiewicz coordinates, are discussed later in this section and are computed using Equations (17) and (16), respectively [9]. Several geometric-optics BRDF models like these exist, albeit having different scalar BRDF forms, including Priest-Germer [10], Beard-Maxwell [11], Sandford-Robertson [1], and others [12, 13, 14, 15, 16, 17], which Butler categorizes to investigate the model terms [8].

The geometric attenuation term was added to these models to account for the divergence of the cross-section conversion term at high incident or scattered angles. There are many different forms used in the various microfacet models. A common

geometric attenuation term, derived by Blinn uses the equation [13]

$$G(\theta_i, \theta_s) = \min\left[1, \frac{2\cos\theta_h\cos\theta_s}{\cos\theta_d}, \frac{2\cos\theta_h\cos\theta_i}{\cos\theta_d}\right],\tag{14}$$

where the minimum of the three expressions is used as the value for each θ_s. The first term represents no geometric attenuation, the second representing geometric attenuation due to obscuration, and the third representing geometric attenuation due to shadowing. This term has a maximum value of 1 due to the min function in Equation (14), but approaches 0 at grazing angles (θ_i approaching $90°$ or θ_s approaching $90°$) due to the cosine term in the denominator. This term is a geometric approximation that ignores diffraction effects, but replacing it with a term that approximates wave optics attempts to fix this issue. Distribution functions can either be isotropic, meaning its dependence is only on θ_i, θ_s, ϕ_s (and thus only θ_h and not ϕ_s) or anisotropic, which additionally depend on ϕ_h. In this work, the surfaces are assumed to be isotropic. These must be normalized so that the integral over the entire hemisphere is 1. Several different distribution functions have been used in the various microfacet models, some common ones being cosine lobe, Gaussian, and Hyper-Cauchy distributions.

$\sigma(\theta_i, \theta_s)$ is the cross-section conversion term, which converts from spherical to planar scattering. The cross-section conversion term is defined specifically as

$$\sigma(\theta_i, \theta_s) = \frac{1}{4\cos\theta_i\cos\theta_h}.\tag{15}$$

The half-angle (θ_h) and difference angle (θ_d) are computed using [9]

$$\cos(2\theta_d) = \cos\theta_i\cos\theta_s + \sin\theta_i\sin\theta_s\cos\phi_s\tag{16}$$

9

$$\cos\left(\theta_h\right) = \frac{\cos\theta_i + \cos\theta_s}{2\cos\theta_d} \tag{17}$$

In vector form, these equations are [9]

$$\hat{\boldsymbol{\omega}}_{\boldsymbol{d}} = \mathbb{R}_y(-\theta_h)\mathbb{R}_z(-\phi_h)\hat{\boldsymbol{\omega}}_{\boldsymbol{i}} \tag{18}$$

$$\hat{\boldsymbol{\omega}}_{\boldsymbol{h}} = \frac{\hat{\boldsymbol{\omega}}_{\boldsymbol{i}} + \hat{\boldsymbol{\omega}}_{\boldsymbol{s}}}{||\hat{\boldsymbol{\omega}}_{\boldsymbol{i}} + \hat{\boldsymbol{\omega}}_{\boldsymbol{s}}||}, \tag{19}$$

where $\hat{\boldsymbol{\omega}}_{\boldsymbol{d}}$, the difference vector, is the rotated incident vector in microsurface coordinates, and $\hat{\boldsymbol{\omega}}_{\boldsymbol{h}}$, the halfway vector, is the specular microsurface orientation. The $\mathbb{R}$ symbol denotes a right-hand rotation about the axis listed as the subscript. The halfway vector is the vector halfway between the incoming and scattered rays, while the difference vector is the incident vector for a frame of reference where the halfway vector is at the surface normal vector. These are illustrated in Figure 1. The **n** and **t** represent the normal and tangent axes, respectively. For the same incident and scattered rays, $\hat{\boldsymbol{\omega}}_{\boldsymbol{i}}$ and $\hat{\boldsymbol{\omega}}_{\boldsymbol{s}}$, both parameter representations are given. Note that Figure 1 neglects ϕ_i, ϕ_s, and ϕ_h, as this work assumes surfaces to be isotropic.

In this work, the volumetric term will not be considered as many models neglect to include it. More research needs to be done on volumetric terms in the microfacet model before those terms are considered. The microfacet model uses the idea that a surface has many small microfacets that make up the roughness of the surface. Each microfacet uses Snell's law of reflection where the angle of the incident light is equal to the angle of the reflected light. Each microfacet has its own normal unit vector where the microfacets are assumed to be symmetrically distributed based on the distribution function chosen. Despite their simplicity, the microfacet model can be improved by approximating ideas from wave optics. One approximation is to replace the Fresnel reflectance term with the Rayleigh-Rice polarization factor, Q.

An approximation was proposed by Butler to relate Fresnel reflectance, G, and σ

10
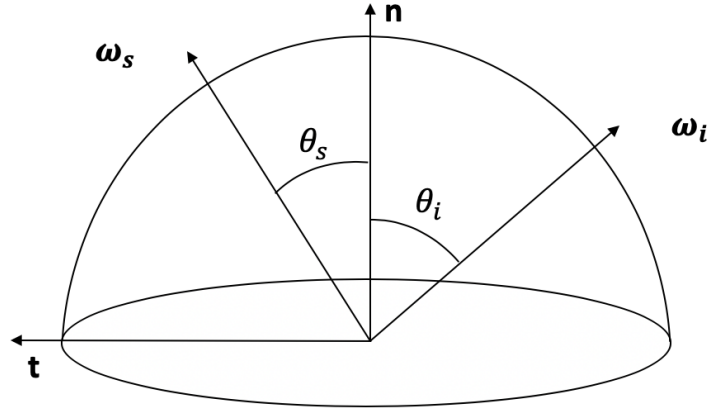
(a) BRDF representation as a function of incident and scattered angles
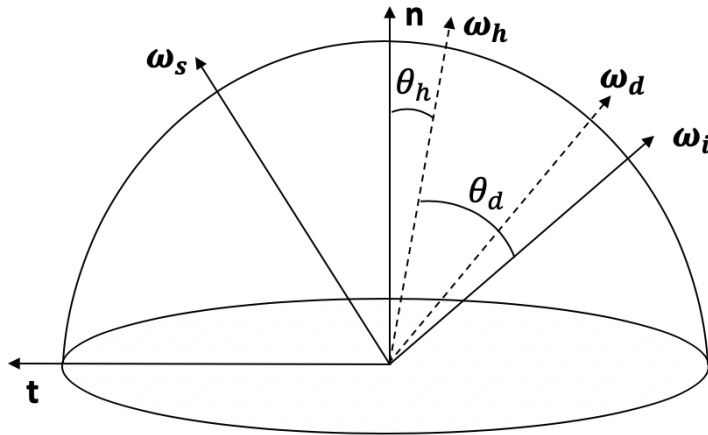
(b) BRDF representation as a function of half-angle and difference angles

Figure 1. Using the half-angle (θ_h) and difference angle (θ_d) condenses the number of parameters needed to physically represent the BRDF

to the Rayleigh-Rice polarization factor, Q [3], as is discussed in the next section.

2.4 Rayleigh-Rice Polarization Factor

The Rayleigh-Rice polarization factor, Q, is more computationally complex, but due to its ties to diffraction theory, it is more physically accurate. Q is broken up into four different polarization states, $Q_{ss}, Q_{sp}, Q_{ps}, Q_{pp}$, where the first subscript is

11

the incident polarization and the second subscript is the scattered polarization. Each of these terms is defined as

$$Q_{ss} = \left| \frac{[\tilde{n}_2^2 - 1] \cos(\phi_s - \pi)}{[\cos \theta_i + \sqrt{\tilde{n}_2^2 - \sin^2 \theta_i}][\cos \theta_s + \sqrt{\tilde{n}_2^2 - \sin^2 \theta_s}]} \right|^2 \tag{20}$$

$$Q_{sp} = \left| \frac{[\tilde{n}_2^2 - 1] \sqrt{\tilde{n}_2^2 - \sin^2 \theta_s} \sin(\phi_s - \pi)}{[\cos \theta_i + \sqrt{\tilde{n}_2^2 - \sin^2 \theta_i}][\tilde{n}_2^2 \cos \theta_s \sqrt{\tilde{n}_2^2 - \sin^2 \theta_s}]} \right|^2 \tag{21}$$

$$Q_{ps} = \left| \frac{[\tilde{n}_2^2 - 1] \sqrt{\tilde{n}_2^2 - \sin^2 \theta_i} \sin(\phi_s - \pi)}{[\tilde{n}_2^2 \cos \theta_i + \sqrt{\tilde{n}_2^2 - \sin^2 \theta_i}][\cos \theta_s + \sqrt{\tilde{n}_2^2 - \sin^2 \theta_s}]} \right|^2 \tag{22}$$

$$Q_{pp} = \left| \frac{[\tilde{n}_2^2 - 1][\tilde{n}_2^2 - \sin^2 \theta_i] \sqrt{\tilde{n}_2^2 - \sin^2 \theta_s} \cos(\phi_s - \pi) - \tilde{n}_2^2 \sin \theta_i \sin \theta_s}{[\tilde{n}_2^2 \cos \theta_i + \sqrt{\tilde{n}_2^2 - \sin^2 \theta_i}][\tilde{n}_2^2 \cos \theta_s + \sqrt{\tilde{n}_2^2 - \sin^2 \theta_s}]} \right|^2 \tag{23}$$

$$Q_{unp} = Q_{ss} + Q_{sp} + Q_{ps} + Q_{pp} \tag{24}$$

As will be discussed in Chapter III, the data in this thesis contains polarimetric BRDF values for various incident angles. In modeling this data, these Q_{xx} terms are used in the equation for the model where the Rayleigh-Rice polarization factor is substituted for the Fresnel, geometric attenuation and cross section conversion terms.

To understand how the replacement is possible, in previous work, Butler developed a relationship between the Fresnel and geometric attenuation terms to the Rayleigh-Rice polarization factor, Q [3]. From comparing the microfacet and wave optics theory BRDF models in a previous work, this relationship between the Fresnel and Rayleigh-Rice term was found to be

$$S = \frac{4 \cos \theta_i \cos \theta_s \cos^4 \theta_h}{(\cos \theta_i + \cos \theta_s)^2} \approx \frac{2F}{Q}, \tag{25}$$

where the Q is the unpolarized Q. To remedy the problem caused by the geometric

term at grazing, or high incident angles, the S approximation was solved for G, [2, 4]

$$G \approx \frac{SQ}{2F} = \frac{4\cos\theta_i \cos\theta_s \cos^4\theta_h}{(\cos\theta_i + \cos\theta_s)^2} \frac{Q}{2F}. \tag{26}$$

This model was found to maintain the computational simplicity of the microfacet model, while diminishing the problematic geometric attenuation term and adding in ideas from wave optics with the Rayleigh-Rice polarization factor. When put together in the microfacet BRDF model, the equation is given as

$$f = \rho_s \cdot D(\theta_h) \cdot \left(\frac{Q}{2}\right) \cdot \left[\frac{1}{(\cos\theta_i + \cos\theta_s)^2}\right] + \frac{\rho_d}{\pi} \tag{27}$$

which was found by Ewing to produce the most accurate BRDF data fit in the grazing angle region. This model will be compared for each polarization state, specifically, Q_{ss}, Q_{pp}, Q_{sp}, and Q_{ps} substituted in for Q to compare to the corresponding raw data [4].

The microfacet distribution of focus for the models considered is the Hyper-Cauchy function, chosen because it can approximate both Gaussian and Lorentzian curves [15]. Ewing also found that for this particular model, the most accurate distribution function for 11 of 18 materials tested was the Hyper-Cauchy distribution. Compared to the Beckmann-Gaussian microfacet surface normal distribution used in the Standard Cook-Torrance model, and the two dimensional surface scatter power spectral density given by Krywonos, the Hyper-Cauchy distribution model fit best to the 18 materials tested [4]. The Hyper-Cauchy distribution function has the form [15]

$$D_h(\theta_h) = \frac{(q-1)(s\sqrt{2})^{2q-2}}{\pi \cos^4\theta_h[(s\sqrt{2})^2 + \tan^2\theta_h]^q}. \tag{28}$$

where s and q are two fitting parameters. When $q = \frac{3}{2}$ in this function, the Cauchy distribution results.

13

III. Methodology and Materials

In order to determine how well the Rayleigh-Rice polarization factor and geometric attenuation term approximation fit polarized BRDF data, each polarization case was coded into MATLAB® and used with the `lsqcurvefit` command, which solves nonlinear data-fitting problems using the least-squares sense. For the Rayleigh-Rice polarization factor, the parameters that were allowed to float were ρ_s, ρ_d, n, κ, and q and s from the Hyper-Cauchy distribution function. Data collected from the Air Force Research Lab Materials and Manufacturing Directorate, Optical Measurements Facility (OMF) is used to compare each model. These data sets obtained scatter data in middle wavelength infrared (MWIR), long wavelength infrared (LWIR), near infrared (NIR), ultraviolet (UV), and visible (VIS) parts of the spectrum for various glossy, diffuse and NIST standard materials. While these same materials were used in previous works to investigate the accuracy of this improved model with wave-optics approximations, not all materials considered in that work were used here [4]. In all, only 14 of the 18 materials in this data set were considered, with the italicized material names not being considered in this thesis. Table 1 shows all 18 materials.

Table 1. 14 materials were used with the novel model across five wavelengths, the four materials shown in italics had issues within the data sets and were not used in this analysis

LWIR ($10.6\mu m$)	**MWIR** ($3.39\mu m$)	**NIR** ($1.06\mu m$)	**VIS** ($0.6328\mu m$)	**UV** ($0.325\mu m$)
PNT 65	PNT 65	PNT 65	PNT 65	PNT 65
PNT 66	PNT 66	PNT 66	*PNT 66*	PNT 66
PNT 00818	STD 00696	36375	36495	
	STD 00698	PNT 01006		
	STD 00699	PNT 01014		

The materials that were omitted either had differing step sizes between different incident angles of the same material, which was the case for PNT 66 and PNT 0818

14

or were missing polarization data, which was the case for STD 00698. Polarization data was taken for all of *ss*, *sp*, and *pp* polarizations, with *ps* taken in some cases. A typical set of BRDF data is shown in Figure 1. The top line is the *ss* polarization, the second highest is the unpolarized data, the third line is the pp polarization, and the *ps* polarization data is one to two orders of magnitude below the other polarization states.
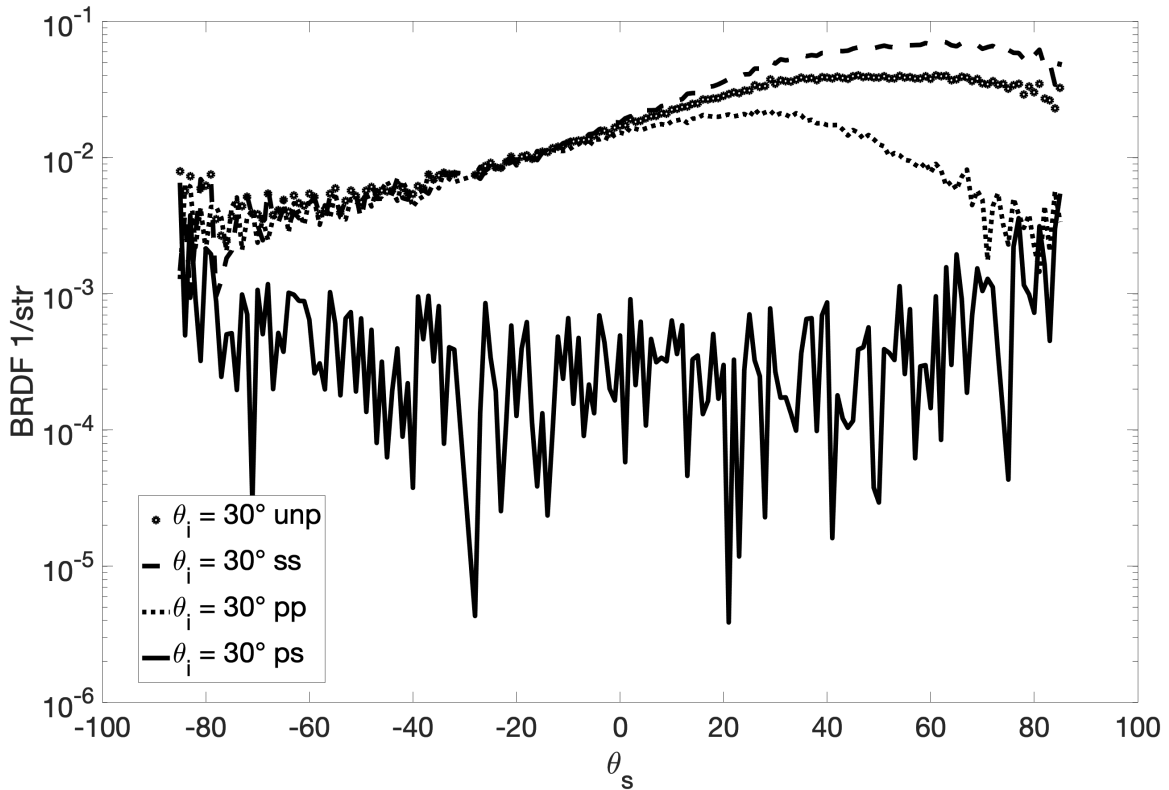
Figure 2. PNT 66 MWIR plot of unpolarized, ss, pp, and ps polarizations

Due to *sp* and *ps* data being too low in magnitude to properly be fitted, these polarization cases are left for future work. The following discussion is only for *ss* and *pp* polarization cases; the methodology for the analysis on these is both the same with the only difference between the two being the Rayleigh-Rice polarization factor. Each material has BRDF data taken for between two to five different incident angles, and there is a set of parameters fitted for each incident angle for each material. In order

15

to use `lsqcurvefit`, lower and upper bounds and an initial guess must be given for the parameters to get the most accurate fit.

The fits of some materials were affected more than others by the backscatter data. This data occurs at reflected angles at 0 degrees and negative angles, meaning light that is reflected back in the incident direction. Since the backscatter region was not an area of interest for this investigation, these angles were neglected. For these data sets, data was truncated to show only positive reflection direction angles. For ss parameters, the data that was truncated was PNT 65 NIR. For pp parameters, PNT 65 NIR, PNT 65 VIS, and PNT65 UV were truncated.

An issue can occur if the initial guess or bounds do not allow for the best combination of parameters to fit the data. To remedy this, a MATLAB® script that randomly generated initial parameter guesses within the lower and upper bounds was written. The bounds used to generate the initial guesses in the final fitting code are in Table 2. The diffuse fitting parameter, ρ_d is definitely only a value between these bounds, as in Equation (13), this value is divided by π and added, not multiplied to the other terms in the BRDF equation. This parameter scales the fitted curve directly up or down on the y-axis. The specular fitting parameter, ρ_s was allowed to vary between 0 and 1000, as a value above this upper bound would not be expected. The model is affected by this parameter through direct scaling, since this term is directly multiplied to the others. The Hyper-Cauchy distribution function fitting parameters, s and q share the upper bound of 10, but q has a minimum of 1.5 due to how values below this cause Equation (28) to not be a realizable number. A higher q value raises the specular peak of the BRDF model curve, while a higher s value lowers the peak by widening the curve. The index of refraction parameters, n and κ also shared a maximum of 100, but the minimum of n was set to 1, as the incident light is assumed to be coming from air, which has an index of refraction of 1. While the minimum for

16

κ is set to 0, κ is typically > 0 since light is absorbed, but $\kappa = 0$ means that light travels forever without loss.

Table 2. Lower and upper bounds for each parameter that were used to generate random sets of parameters that best fit polarization data

ρ_d	ρ_s	s	q	n	κ
0	0	0	1.5	1	0
1	1000	10	10	100	100

Running the curve fitting scheme with at least a hundred iterations of random initial guesses allows for the global, not just local, minimum error to be determined for each data set. This global minimum for the initial guess should theoretically be the same logarithmic error that the curve fitted parameters yield, as the curve fit with this initial guess should be as good, if not better than the initial guess. This is important because it allows for the best combination of parameters to be found, rather than prematurely stopping when a local minimum is determined. Within those hundred iterations, the combination of parameters with the absolute lowest logarithmic error are found for each incident angle. These sets of parameters represent the cases where the randomized initial parameters best fit the data, and are used for the initial guesses for the curve fitting code for each material. In all cases, the initial guesses for parameters that provided the absolute lowest error for the incident angle of a material were used.

The accuracy of each of these fits was determined using an error analysis and comparing the size of the errors between the fitted parameters and the material data. The logarithmic error is calculated for each material's incident angle within the MATLAB® code in the same way as in [4] as

$$\delta = \frac{1}{n} \sum_{k=1}^{n} |\ln x_k - \ln f_k|, \tag{29}$$

17

where x is the natural logarithm of the BRDF data being fitted and f is the natural logarithm of the model with the fitted parameters. The natural logarithm metric is used in this equation so that the specular peak of the data sets is not over-emphasized when calculating the error over the whole data set [4].

After finding values for parameters for each incident angle for each material, these parameters were used on other data, namely ss parameters were used on pp and unpolarized data and pp parameters were used on ss and unpolarized data. The reason for investigating this is to determine how different the parameters really are, if one set of parameters can be used for one material or if it is just limited to its polarization case. The accuracy in these cases is calculated in the same way as above.

Plots of the fitted model on the data for both ss and pp polarization are shown in the results section, along with the fitted parameters that were calculated using the MATLAB® code. Following these figures, plots of the ss parameters plotted on pp data are presented $(ss-pp)$. Similarly, pp parameters used with the ss Rayleigh-Rice polarization in the BRDF model are shown on ss data $(pp-ss)$. In the same way, both ss and pp parameters are shown on unpolarized data $(ss-unp$ and $pp-unp)$.

IV. Results and Analysis

4.1 Introduction

As mentioned in the previous section, at least a hundred iterations of initial guesses were calculated for each material. The initial guesses with the overall lowest value for each incident angle of the material were used as the initial guess for the subsequent curve fit. For each material, the plots of the *pp* and *ss* polarized data fits are presented, followed by the tables of the *pp* and *ss* fitted parameters. These tables also include a row of unpolarized parameters from a previous study to compare with the polarized cases [2]. Unpolarized parameters were calculated from fitting all material data, but the logarithmic data from these is not readily available. For each material, the cross-term comparisons are shown, first with plots of the four cases and then with a table displaying the logarithmic error for all cases for each incident angle. Discussion of the fitted parameters and the cross-terms cases are presented in the following Analysis section.

4.2 PNT 65

Figure 3 shows the plots of the PNT 65 LWIR data, modeled with fitted parameters for each incident angle and with a global set of parameters that apply to all incident angles. Parameters were found for both 30° and 60°, but a set of parameters that were fitted to data of both angles were found to better represent each material individually. Since these "all" parameters are more general, there is a higher error when using them to fit the data with the model.
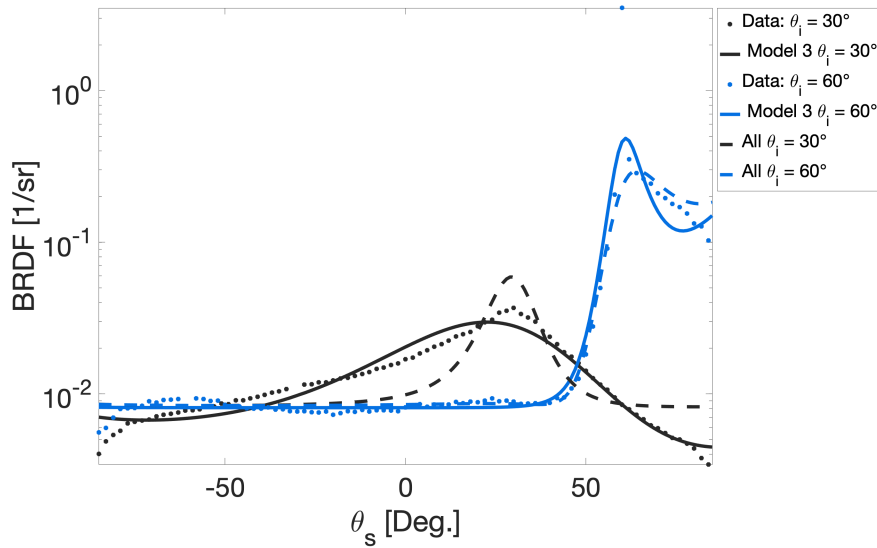
(a) PNT 65 LWIR pp polarization
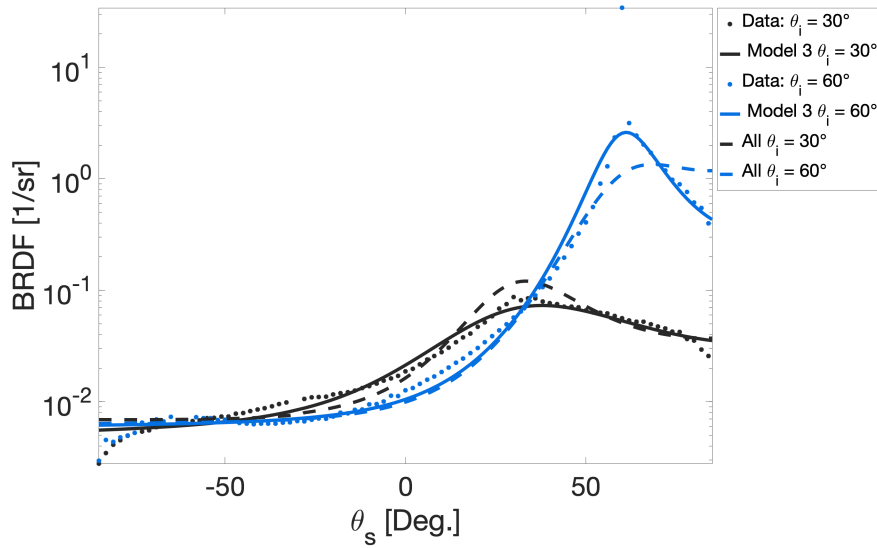
(b) PNT 65 LWIR ss polarization

Figure 3. The paint labeled PNT 65 in the LWIR was better fit in the pp polarization than in the ss polarization. The model was fitted to each incident angle individually and then for all angles to generate a single set of parameters that represent this material.

Tables 3 and 4 show the parameters determined from both incident angles individually and the parameters from fitting all of the data. The logarithmic error is

20

calculated using Equation (29). The lower incident angle for both polarizations has a lower logarithmic error, while the higher incident angle has a higher logarithmic error. Of note in Table 3 is that κ is 0 for the 30° case and n is 1 for the 60° case, which are both values that are not representative of what is expected. For both incident angles in the *ss* case, the index of refraction is 1, and the attenuation coefficient, κ is at its upper bound of 100 for the higher incident angle case. Similarly, in both tables, one of the Hyper-Cauchy values, q is at its lower bound of 1.5 for 60° incident angle. While the model does fit the data with these parameters, the specular peak in both cases can be seen to be slightly problematic, thus resulting in these non-realizable parameters.

Table 3. PNT 65 LWIR pp parameters that are fitted to all of the data better match 60° than 30°. ρ_d and κ of the 'all' parameters and 60° compare well with unpolarized parameters.

θ(deg)	ρ_d	ρ_s	s	q	n	κ	Log. Error
30	0.012	3.899	0.260	2.246	1.367	0.000	0.0111
30 (All)	0.026	0.888	0.056	1.584	1.354	0.038	0.1180
60	0.025	0.021	0.032	1.500	1.000	0.029	0.0176
60 (All)	0.026	0.888	0.056	1.584	1.354	0.038	0.1279
Unpol	0.02	1	0.1	1.5	1.5	0.2	

Table 4. PNT 65 LWIR ss parameters consistently hit the minimum values for q and n, and 60° hits the maximum value for κ. The unpolarized index of refraction being different suggests that the ss Rayleigh-Rice factor needs more development.

θ(deg)	ρ_d	ρ_s	s	q	n	κ	Log. Error
30	0.015	0.509	0.218	1.902	1.000	0.971	0.0117
30 (All)	0.018	1.450	0.115	1.500	1.000	0.453	0.1249
60	0.019	0.276	0.066	1.500	1.000	100.000	0.0226
60 (All)	0.018	1.450	0.115	1.500	1.000	0.453	0.1199
Unpol	0.02	1	0.1	1.5	1.5	0.2	

Table 5 displays the logarithmic error terms for each of the cross term cases. For

21
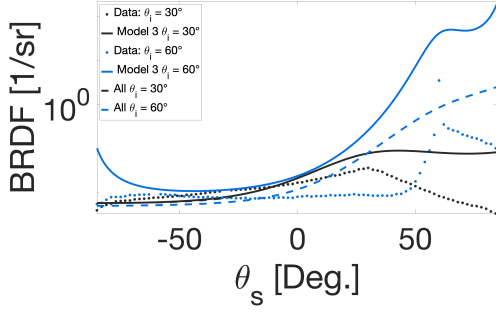
(a) PNT 65 LWIR ss on pp data
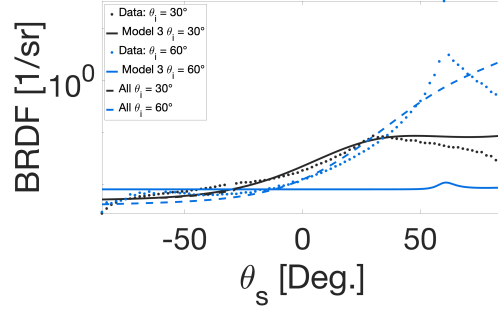
(b) PNT 65 LWIR pp on ss data
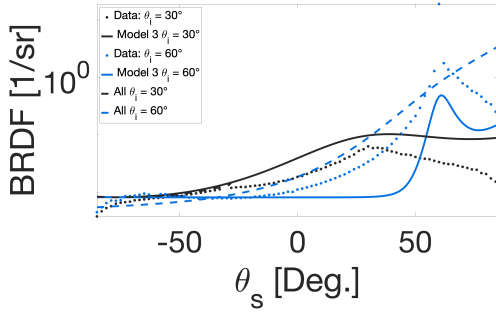
(c) PNT 65 LWIR pp on unpolarized data
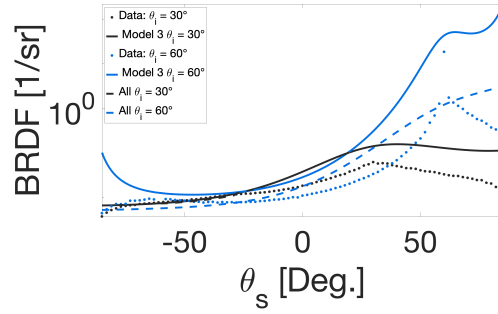
(d) PNT 65 LWIR ss on unpolarized data

Figure 4. PNT 65 LWIR fits the lower incident angle data with less error in all cases

each incident angle, 30° and 60° for the case of PNT 65 LWIR, the calculated error, using Equation (29) is reported. Each case represents the fitted ss and pp polarization parameters, either from Table 3 or Table 4 for the case of PNT 65 LWIR and inputted into the model to fit to the opposite polarization or unpolarized data. For instance, ss parameters are used in Q_{ss} in the model for the $ss - ss$ case, in Q_{pp} in the $ss - pp$ case, and in Q_{unp} in the $ss - unp$ case.

The $ss - ss$ column represents the parameters reported in Table 4 plotted on ss polarization data, plotted in Figure 3(b). The $ss - pp$ column represents the parameters from Table 4 plotted on pp polarization data, as represented in Figure 4(a). The $ss - unp$ column takes the parameters from Table 4 and plots the model on unpolarized data, which is shown in Figure 4(d). The $pp - pp$ column represents pp parameters from Table 3 plotted on pp polarization data, which is shown plotted

22

Table 5. PNT 65 LWIR Polarization Term Error from the cross-term polarization fits show that pp parameters fit pp, ss, unpolarized data in all cases except for 30 (All)

θ	ss-ss	ss-pp	ss-unp	pp-pp	pp-ss	pp-unp
30	0.0117	0.0996	0.0699	0.0111	0.0267	0.0557
30 (All)	0.1249	0.1021	0.0934	0.1180	0.1063	0.0992
60	0.0226	0.2540	0.1849	0.0176	0.1967	0.0824
60 (All)	0.1199	0.2222	0.1637	0.1279	0.1208	0.1491

in Figure 3(a). Similarly to the ss polarization case, $pp - ss$ means that the pp parameters are plotted on ss polarization data, shown plotted on Figure 4(b). Finally, the error resulting from fitting pp parameters plotted on unpolarized data is shown in the $pp - unp$ column, with the plot in Figure 4(c).

All figures show the data with parameters fitted to each incident angle (solid lines) and with a single set of parameters fitted to all the data (dashed line). Each incident angle is represented by its own color and will have an optimized fit and an 'all' fit. The errors shown in Table 5 compile the logarithmic error for all of the cases, where a lower number means there is less error. Each material follows this framework, and short descriptions of the material performance follow the figures and tables.

For the PNT 65 MWIR case, the fit has half the error for the lower incident angle case, shown in Figure 5. For the higher incident angle case, the error of the model fits are comparable. There are concerns with how the fitting routine achieves its lowest error value. In the pp polarization case, both the κ terms are 0, which, as previously mentioned, is not physically accurate for a paint. Similarly, the ss polarization case fitted the n value to 1 for both incident angles, which is approximated to be air or a conductor. Since the assumed incident material was air, the n value for the paint should not be the same as the incident case, but it is acceptable for κ to be a large value. Between the ss and pp parameters, there doesn't seem to be any trend or relation between the fit parameters.

23
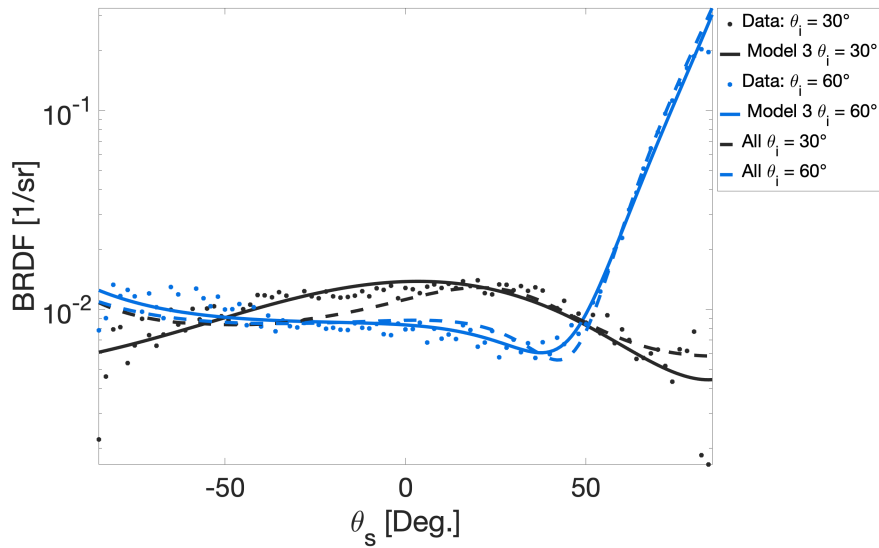
(a) PNT 65 MWIR pp polarization
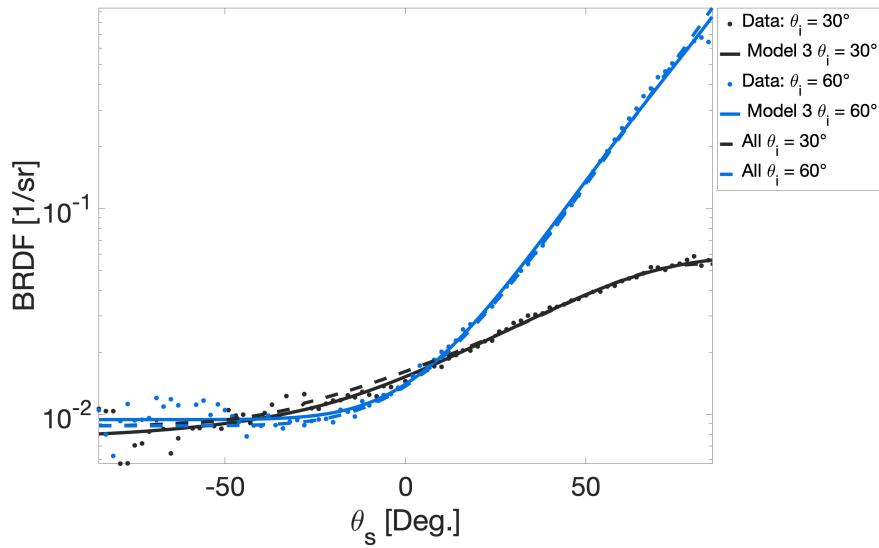
(b) PNT 65 MWIR ss polarization

Figure 5. PNT 65 MWIR data is well-fitted by the model, both for the separate incident angle parameters and the 'all' parameters. The model fails to fit data in the backscatter region and at high scattered angles.

Comparing all of the cross term cases, the $pp - pp$ and $ss - ss$ both performed the best, while the $ss - pp$ had the highest error in both cases. In the lower incident angle

Table 6. PNT 65 MWIR pp parameters from fitting to data are shown. The "all" parameters are a single set of parameters to represent this material, but perform with much higher error. s and q compare well with unpolarized parameters.

$\theta(\deg)$	ρ_d	ρ_s	s	q	n	κ	Log. Error
30	0.010	3.232	0.643	4.075	1.376	0.000	0.0143
30 (All)	0.017	2.074	0.242	1.570	1.366	0.000	0.0888
60	0.019	1.776	0.285	1.500	1.334	0.000	0.0098
60 (All)	0.017	2.074	0.242	1.570	1.366	0.000	0.0999
Unpol	0.025	0.22	0.22	1.5	2	0.2	

Table 7. PNT 65 MWIR ss parameters match unpolarized parameters for ρ_d, but no other parameters. The model hits the maximum value for q and the minimum value for n, which indicates that the ss Rayleigh-Rice parameter does not perform as well as the pp.

$\theta(\deg)$	ρ_d	ρ_s	s	q	n	κ	Log. Error
30	0.025	1.445	0.515	4.089	1.000	0.321	0.0070
30 (All)	0.028	1.233	0.861	10.000	1.000	0.332	0.0774
60	0.030	0.932	0.823	10.000	1.000	0.404	0.0092
60 (All)	0.028	1.233	0.861	10.000	1.000	0.332	0.0772
Unpol	0.025	0.22	0.22	1.5	2	0.2	

case, the $pp-ss$ case performs better than both the $ss-unp$ and the $pp-unp$ terms, despite the $pp-ss$ and $pp-unp$ having similar data shapes. In the $60°$ case, the pp parameters on unpolarized data appear to fit well in the backscatter region, but do not model the specular peak at all. The pp parameters modeling ss data, on the other hand, fit neither the backscatter nor the specular peak for the $60°$ case. However, in the $30°$ case, the pp parameters on ss data fit better than the pp parameters on unpolarized data. Since this is the only material with reliable data in the LWIR case, a definitive trend cannot be determined as far as the interchangeability of parameters and data, except that ss parameters on pp data are not interchangeable.

For PNT 65, the NIR case was one that needed to be truncated for both pp and ss polarization, as the back-scatter negatively affected the fit, shown in Figure 7. Since

25

(a) PNT 65 MWIR ss on pp data

(b) PNT 65 MWIR pp on ss data

(c) PNT 65 MWIR pp on unpolarized data

(d) PNT 65 MWIR ss on unpolarized data
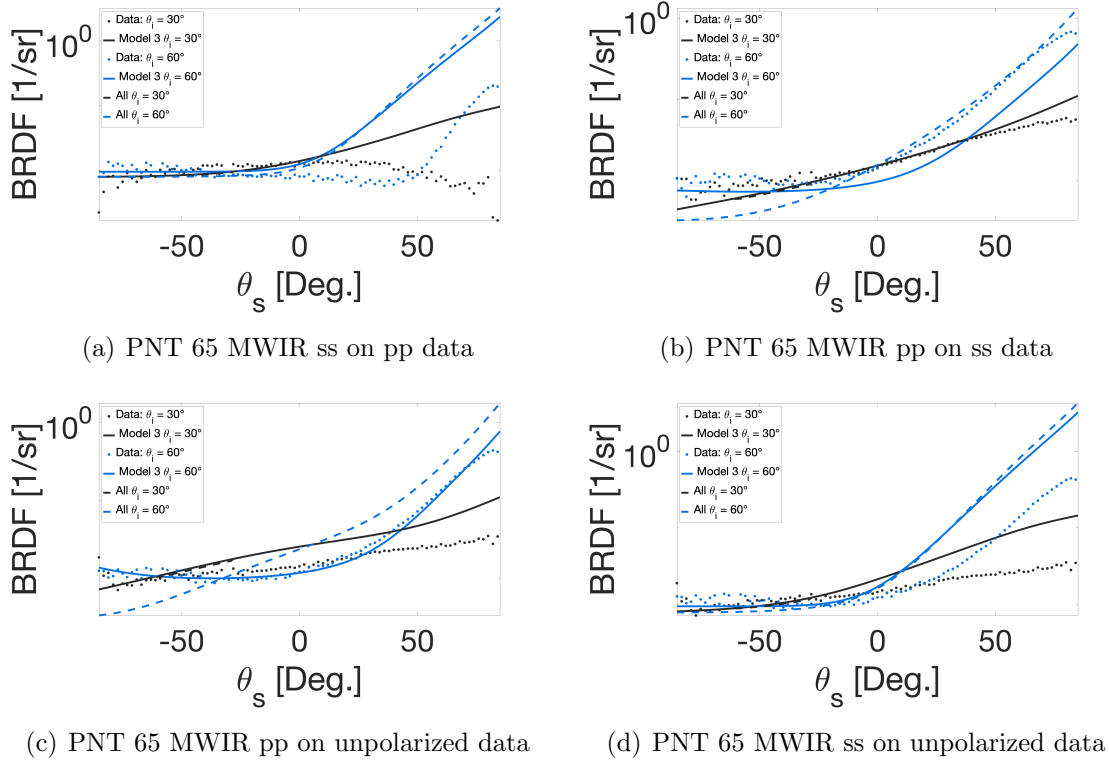
Figure 6. PNT 65 MWIR cross term comparison shows parameters may not be used effectively on other data

Table 8. PNT 65 MWIR polarization term errors show that pp parameters better fit ss, and unpolarized compared to ss parameters on pp and unpolarized. However, $ss - ss$ has lower error than $pp - pp$ in all cases.

θ	ss-ss	ss-pp	ss-unp	pp-pp	pp-ss	pp-unp
30	0.0070	0.0964	0.0569	0.0143	0.0228	0.0447
30 (All)	0.0774	0.0992	0.0581	0.0888	0.0681	0.0550
60	0.0092	0.1271	0.0752	0.0098	0.0422	0.0114
60 (All)	0.0772	0.2350	0.1717	0.0999	0.0958	0.1259

the backscatter region is not the main region of interest in this study, truncating the data at 0° is sufficient to get the fitted parameters. Again there are some issues with the indices of refraction for both pp and ss and both incident angles, as shown in Tables 9 and 10. Despite this, the logarithmic error for these cases are among the lowest, likely due to the the truncation, shown in Table 11. Also in this wavelength

region, the data more tightly converges to a straight line than, say PNT 65 MWIR data, where the backscatter data was more scattered.
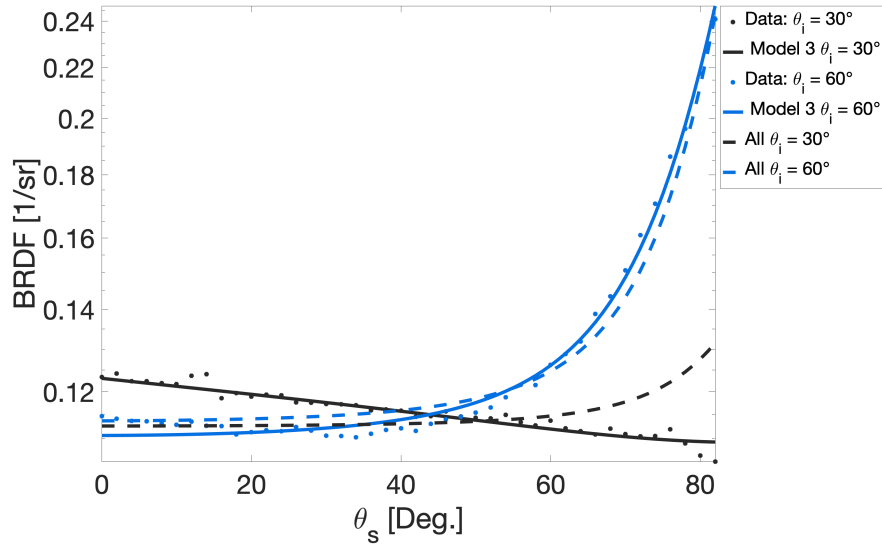
(a) PNT 65 NIR pp polarization
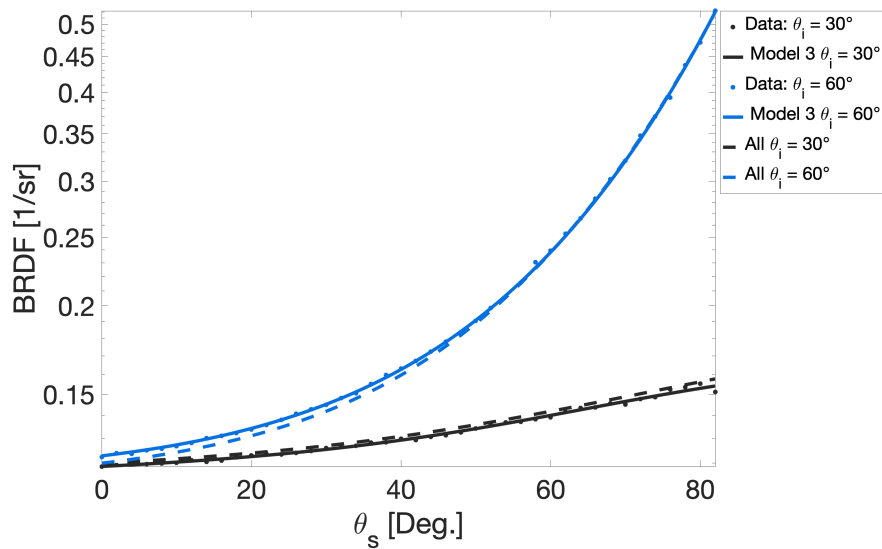
(b) PNT 65 NIR ss polarization

Figure 7. PNT 65 NIR was truncated in both the pp and ss polarization, which allowed for lower error compared to other materials. The 'all' parameters fit the best in the $60°$ case, but struggle in the $30°$ case in the pp polarization at scatter angles higher than $60°$

27

Table 9. PNT 65 NIR pp parameters do not correspond well with any of the unpolarized parameters. ρ_d and n are consistent among the polarized parameters, but an n of 1 hits the lower bound for three of the four cases.

θ(deg)	ρ_d	ρ_s	s	q	n	κ	Log. Error
30	0.340	9.299	1.113	4.933	1.361	0.000	0.0015
30 (All)	0.353	0.061	4.175	5.450	1.000	4.476	0.0205
60	0.340	6.112	9.976	1.501	1.001	3.186	0.0020
60 (All)	0.353	0.061	4.175	5.450	1.000	4.476	0.0241
Unpol	0.7	1.7	1.2	2	1.2	0.2	

Table 10. PNT 65 NIR ss parameters, like the pp parameters, do not correspond well to the unpolarized parameters. s and q vary between the three sets of parameters, and the only case where n is not 1 has the lowest error, meaning those that are 1 indicate an issue with the ss Rayleigh-Rice term.

θ(deg)	ρ_d	ρ_s	s	q	n	κ	Log. Error
30	0.351	0.746	1.036	9.582	1.001	0.486	0.0007
30 (All)	0.353	0.753	0.819	5.644	1.000	0.552	0.0529
60	0.366	0.692	0.850	7.330	1.741	0.001	0.0006
60 (All)	0.353	0.753	0.819	5.644	1.000	0.552	0.0538
Unpol	0.7	1.7	1.2	2	1.2	0.2	

All cases of PNT 65 NIR were truncated to take away the backscatter that was affecting the quality of the fits. Of all materials PNT 65 NIR $ss - ss$ and $pp - pp$ error terms were the lowest in Table 11. Both incident angles had ss parameters on pp polarization data as the lowest error terms of all of the cases. Figure 8(a) shows that the fits are not entirely accurate, but the 60° case fits closely in the grazing angle region. The $pp - ss$ case also is close in error value to the $ss - pp$ case for the 30° case, and this can be seen in Figure 8(b) where the model at angles around 0° fit closely to the data.

PNT 65 UV was a unique case where the pp polarization data needed to be truncated, while the ss polarization case did not need to be, plotted in Figure 9. In

28

(a) PNT 65 NIR ss on pp data

(b) PNT 65 NIR pp on ss data

(c) PNT 65 NIR pp on unpolarized data

(d) PNT 65 NIR ss on unpolarized data
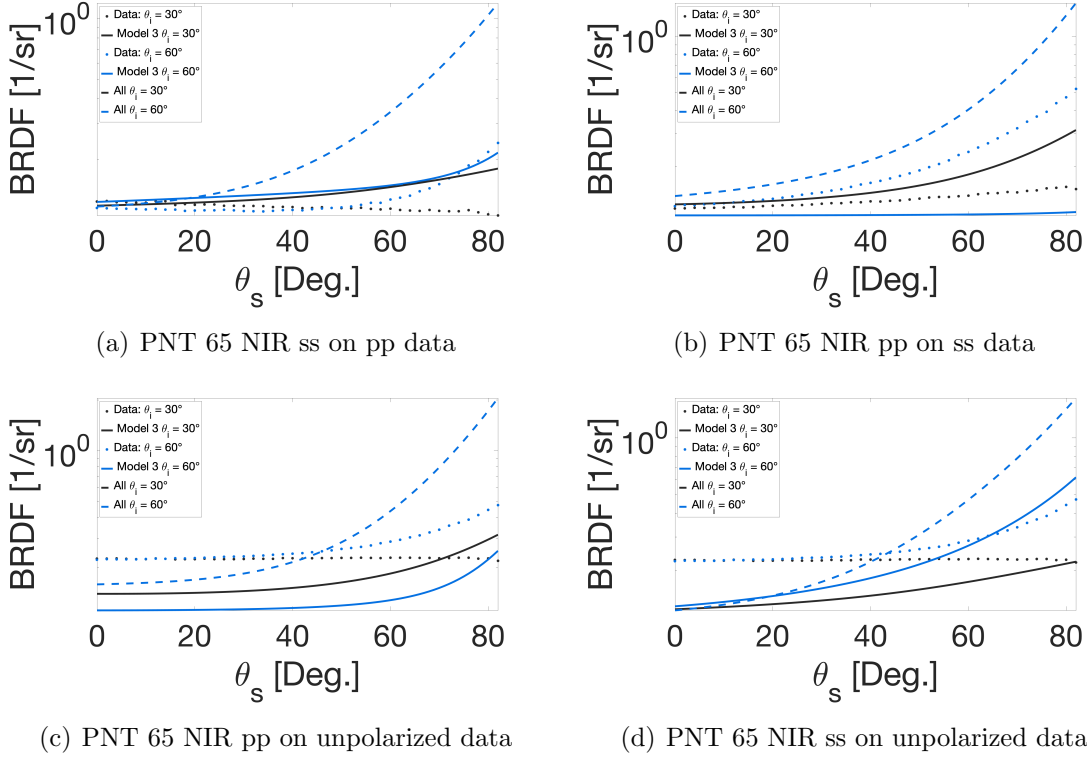
Figure 8. PNT 65 NIR fits have the least error when fitting ss parameters onto pp polarization data

Table 11. PNT 65 NIR polarization term errors show that $ss - pp$ **error are lower than** $pp - ss$**, which doesn't follow the trend of other materials.** $pp - unp$ **error is lower than** $ss - unp$ **parameters in three of the four cases.**

θ	ss-ss	ss-pp	ss-unp	pp-pp	pp-ss	pp-unp
30	0.0007	0.0246	0.0461	0.0015	0.0292	0.0405
30 (All)	0.0529	0.0248	0.0738	0.0205	0.0384	0.0616
60	0.0006	0.0162	0.0366	0.0020	0.0744	0.0816
60 (All)	0.0538	0.1405	0.1075	0.0241	0.1183	0.1061

fact, the ss polarization case had lower logarithmic errors compared to the truncated pp case for both incident angles. This wavelength region did not have any values of κ of 0, but both the ss cases and the 60° case for pp polarization had n values of 1. In both cases, the higher incident angle had a higher error. Also of note is the diffuse fitting parameter for the 60° case as 0. The data for this case starts at a higher value

29

than the 30° case, so it is of interest why this case results in a fitting parameter of 0.
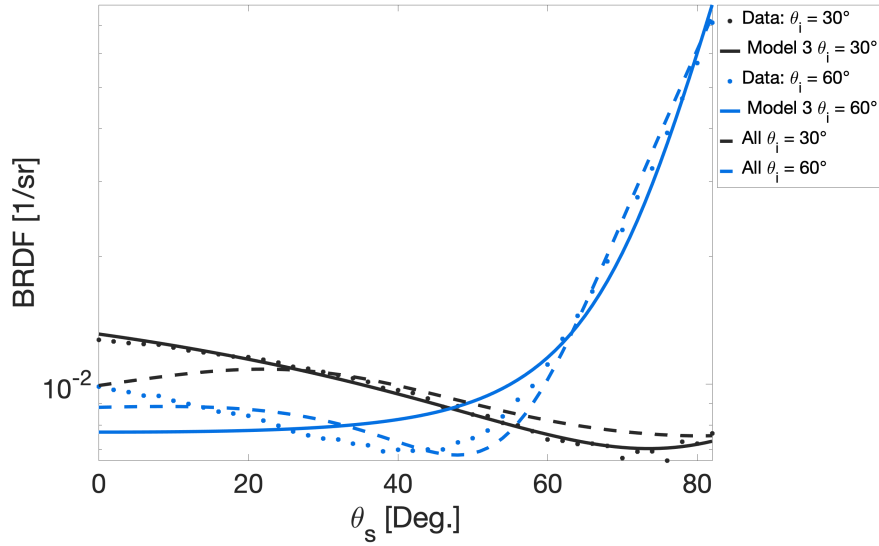
(a) PNT 65 UV pp polarization
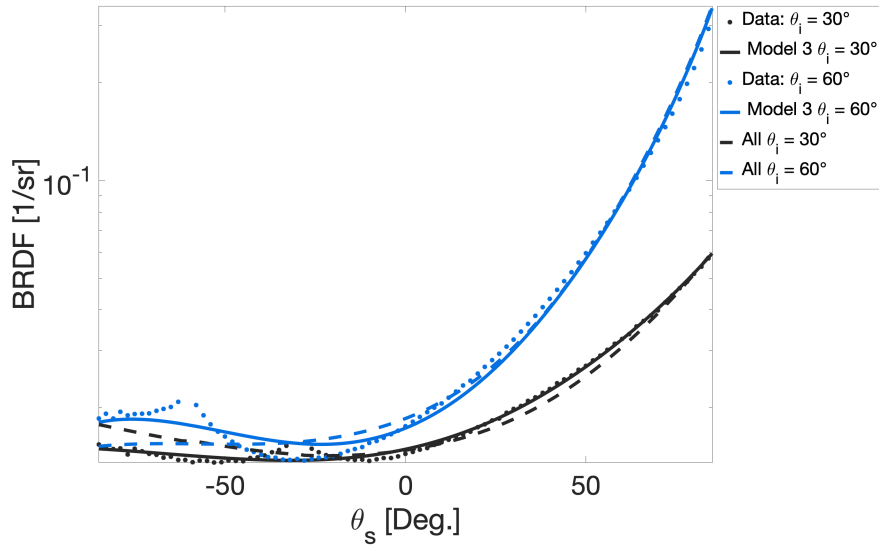
(b) PNT 65 UV ss polarization

Figure 9. PNT UV ss and pp polarization comparison shows that ss fitting has lower error, since the model struggles to reach the dip in the pp polarization. The 'all' plot fits the dip better than the separate 60° fitted model.

As in other material cases, the $ss - ss$ and $pp - pp$ fits have the lowest error, shown

30

Table 12. PNT 65 UV pp parameters are consistent for ρ_d, but do not correspond well to any unpolarized parameters. The 'all' parameters hit the q and κ lower bound, which may indicate that the model has problems optimizing the fit to the data.

θ(deg)	ρ_d	ρ_s	s	q	n	κ	Log. Error
30	0.020	3.447	1.285	8.481	1.337	0.031	0.0026
30 (All)	0.021	1.108	0.250	1.500	1.401	0.000	0.0812
60	0.024	0.030	1.582	8.363	1.000	0.040	0.0148
60 (All)	0.021	1.108	0.250	1.500	1.401	0.000	0.0880
Unpol	0.04	1.7	0.73	2	1.2	0.2	

Table 13. PNT 65 UV ss parameters do not correspond at all to any of the unpolarized parameters. All parameters except ρ_s seem to have consistent values. q and n reach their lower bound in almost all cases, indicating that the model in the ss polarization does not properly optimize the combination of these terms.

θ(deg)	ρ_d	ρ_s	s	q	n	κ	Log. Error
30	0.020	1.409	0.625	1.613	1.000	0.906	0.0023
30 (All)	0.029	2.207	0.585	1.500	1.000	0.556	0.0495
60	0.000	4.011	0.893	1.500	1.000	0.855	0.0054
60 (All)	0.029	2.207	0.585	1.500	1.000	0.556	0.0489
Unpol	0.04	1.7	0.73	2	1.2	0.2	

in Table 14. In the case of PNT 65 UV, each incident angle has a different cross-term error that is the second best. Although an entire order of magnitude higher than the $pp - pp$ case, the $pp - ss$ case is the lowest error for the $30°$ incident angle, while $ss - unp$ is the lowest for the $60°$ case. Figure 10(b) shows how well the $pp - ss$ fit fits for scattered angles around 0 to $40°$. Of all the cross-term cases for PNT 65 UV, $pp - ss$ has the lowest error likely for its fit at those angles.

Similar to the PNT 65 UV case, the VIS pp polarization data was truncated, while the ss polarization data was not, plotted in Figure 11. Actually, the model did attempt to fit the backscatter in the ss polarization case, at least for the $60°$ case. Unlike in the UV case, the truncated data had a lower logarithmic error, while the non-truncated case had slightly higher error. Again, three out of the four cases resulted

31

(a) PNT 65 UV ss on pp data

(b) PNT 65 UV pp on ss data

(c) PNT 65 UV pp on unpolarized data

(d) PNT 65 UV ss on unpolarized data
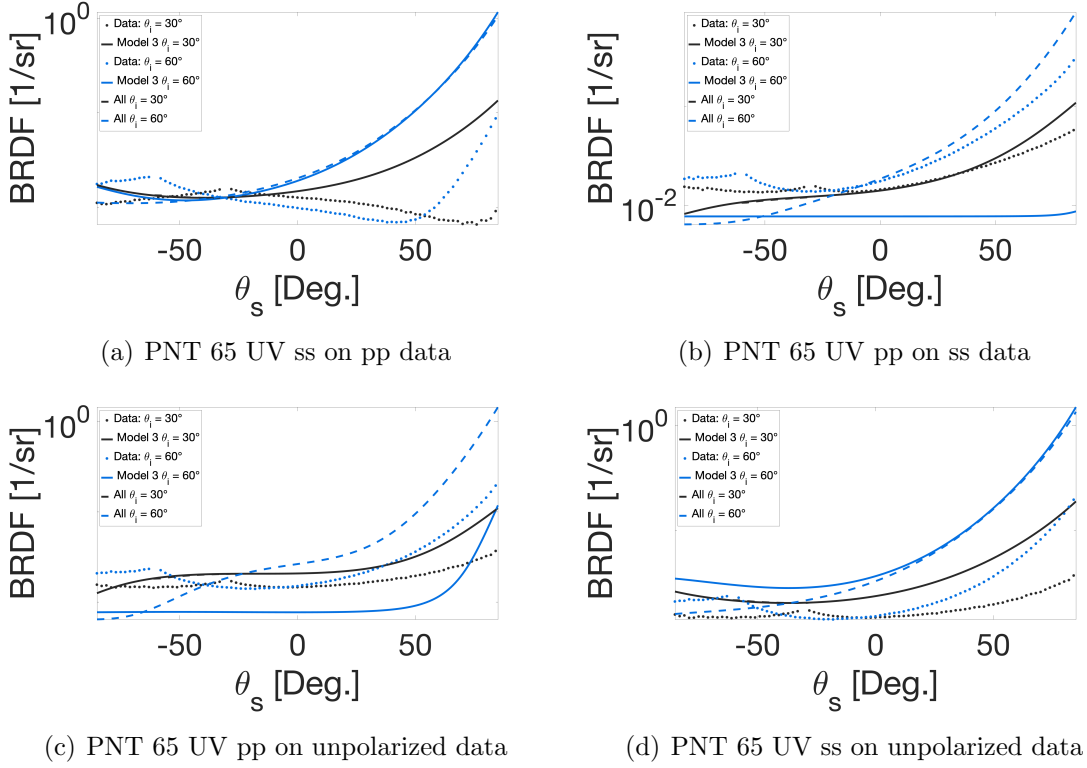
Figure 10. PNT 65 UV best crossterm fit error is an order of magnitude higher than Figure 8 fits

Table 14. PNT 65 UV polarization term error is lowest in the $ss - ss$ cases, but $pp - ss$ has lower error than $ss - pp$ in three of four cases and $pp - unp$ has lower error in all cases.

θ	ss-ss	ss-pp	ss-unp	pp-pp	pp-ss	pp-unp
30	0.0023	0.0834	0.0594	0.0026	0.0201	0.0349
30 (All)	0.0495	0.0976	0.0624	0.0812	0.0433	0.0353
60	0.0054	0.1205	0.0858	0.0148	0.1226	0.0763
60 (All)	0.0489	0.1884	0.1423	0.0880	0.0905	0.1258

in an n of 1, despite knowing that the material has a higher index of refraction. Since the 30° for the ss case does not attempt to fit the backscattered peak, the logarithmic error for the data may be even better than what is reported in Table 17.

PNT 65 VIS has the lowest error for the $pp - ss$ cross term comparisons in Table 17. While this error is an order of magnitude higher than the $ss - ss$ and $pp - pp$

32

cases, it is at least half the value of most of the other cross-term cases. Figure 12(b) shows that while $pp - ss$ has the lowest error the fit is not actually a good fit of the data. In fact, Figure 12(a) 30° appears to be a better fit for the data, but the error is twice as much as the $pp - ss$ comparison.

Table 15. PNT 65 VIS pp parameters do not closely match with any of the unpolarized parameters. ρ_d **is consistent over all cases, but the lower bound for** n **is hit in two of the three parameter sets, including the 'all' parameters.**

θ(deg)	ρ_d	ρ_s	s	q	n	κ	Log. Error
30	0.235	5.181	9.975	1.515	1.359	0.161	0.0026
30 (All)	0.227	0.157	5.714	4.074	1.000	4.067	0.0234
60	0.222	4.413	10.000	1.534	1.000	3.242	0.0021
60 (All)	0.227	0.157	5.714	4.074	1.000	4.067	0.0267
Unpol	0.44	1.7	0.45	1.5	1.2	0.2	

Table 16. Among PNT 65 VIS ss parameters he upper bound for q **is reached, while the 'all' parameters use the lower bound. All cases have** n **as 1, and all of these trends indicate an issue with the ss Rayleigh-Rice parameter.**

θ(deg)	ρ_d	ρ_s	s	q	n	κ	Log. Error
30	0.237	0.713	1.846	10.000	1.000	0.910	0.0037
30 (All)	0.241	5.165	0.750	1.500	1.000	0.409	0.0291
60	0.049	5.361	4.962	10.000	1.000	100.000	0.0036
60 (All)	0.241	5.165	0.750	1.500	1.000	0.409	0.0298
Unpol	0.44	1.7	0.45	1.5	1.2	0.2	
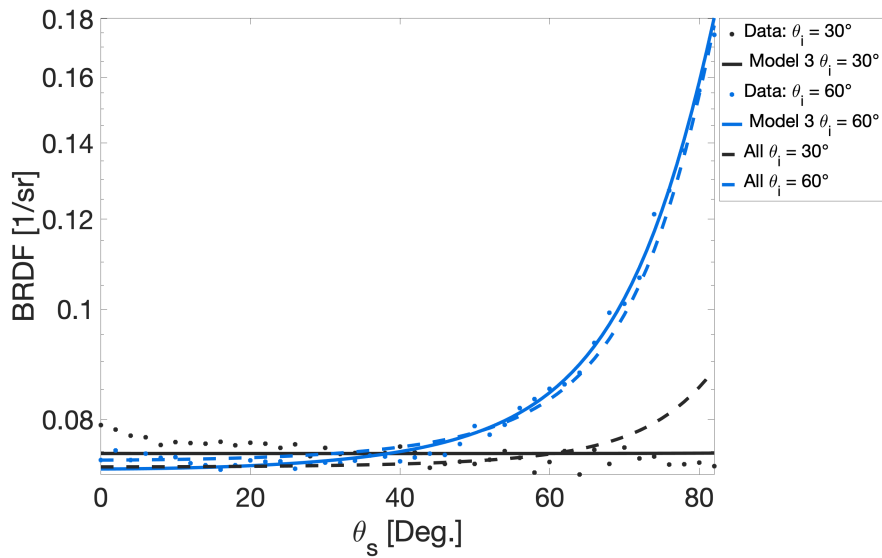
(a) PNT 65 VIS pp polarization
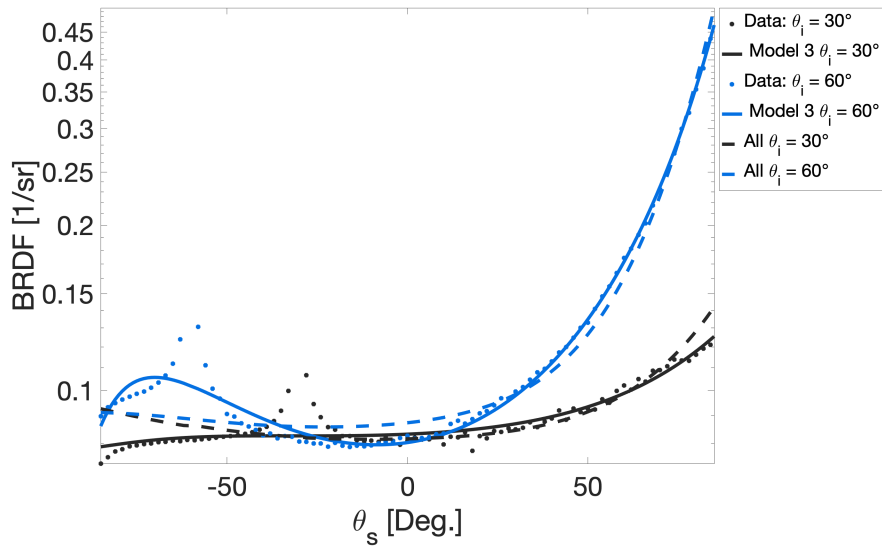
(b) PNT 65 VIS ss polarization

Figure 11. PNT 65 VIS pp and ss polarization are shown side-by-side. The model attempts to fit the backscatter peaks in the ss polarization for 60°. The 'all' parameters in the pp polarization for 30° deviate from data starting at scattered angles for 60°.

34

(a) PNT 65 VIS ss on pp data

(b) PNT 65 VIS pp on ss data

(c) PNT 65 VIS pp on unpolarized data

(d) PNT 65 VIS ss on unpolarized data
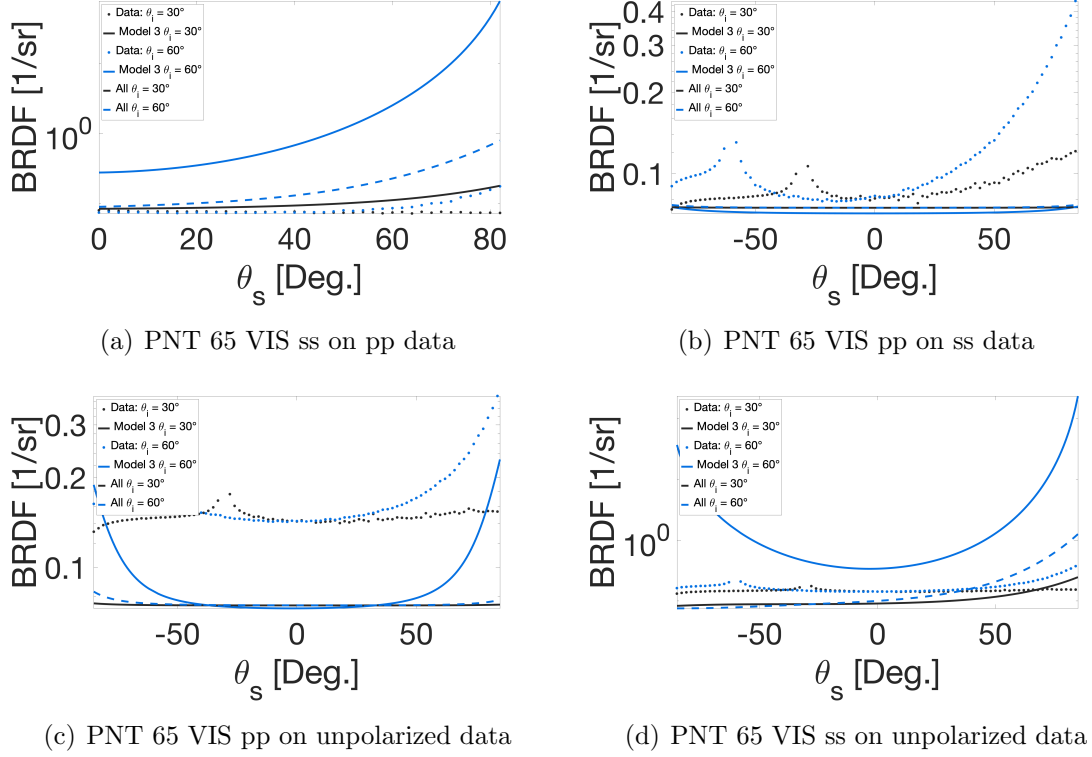
Figure 12. PNT 65 VIS cross term fits are an order of magnitude higher than Figure 10 fits

Table 17. PNT 65 VIS polarization term error shows that $pp - ss$ error is lower in three of four cases, while $ss - unp$ is lower in three of four cases, which does not follow the trend of pp parameters better modelling cross-term polarization.

θ	ss-ss	ss-pp	ss-unp	pp-pp	pp-ss	pp-unp
30	0.0037	0.0414	0.0331	0.0026	0.0155	0.0525
30 (All)	0.0291	0.0452	0.0500	0.0234	0.0472	0.0833
60	0.0036	0.3274	0.1856	0.0021	0.0466	0.0538
60 (All)	0.0298	0.1414	0.0682	0.0267	0.0468	0.0823

4.3 PNT 66

For PNT 66 in the MWIR case, the error in the pp polarization case goes against expectation in that the lower incident angle has the higher error term in Table 18. While the rest of the parameters in this case seem realistic, κ is 0, which may cause

concern about the accuracy of these parameters. However, as with all cases, these parameters did reflect the lowest minimum error over a hundred iterations of initial guesses. The 30° case in the ss polarization has an erroneous term in the index of refraction as in Table 19. The rest of the terms in both these cases seem realistic and are within a magnitude of each other. Plots of PNT 66 MWIR ss and pp polarization are shown in Figure 13.

Table 18. PNT 66 MWIR pp parameters are consistent across cases for all parameters. The 30° case differs the most from the 'all' and 60° parameters, which may indicate that 60° dominates in the 'all' parameters.

θ(deg)	ρ_d	ρ_s	s	q	n	κ	Log. Error
30	0.001	3.455	0.332	2.500	1.399	0.000	0.0169
30 (All)	0.009	2.127	0.302	2.914	1.388	0.030	0.1147
60	0.004	2.642	0.198	1.805	1.403	0.047	0.0145
60 (All)	0.009	2.127	0.302	2.914	1.388	0.030	0.1248
Unpol	0.015	1.7	0.2	1.8	1.2	0.2	

Table 19. PNT 66 MWIR ss parameters hit the lower bound for n for the 'all' parameters and the 30° case. The 'all' and the unpolarized parameter ρ_s are closer than the parameters for each incident angle individually.

θ(deg)	ρ_d	ρ_s	s	q	n	κ	Log. Error
30	0.006	1.035	0.348	2.540	1.000	0.633	0.0175
30 (All)	0.007	1.829	0.319	2.490	1.000	0.428	0.0959
60	0.001	2.560	0.198	1.500	1.646	0.007	0.0188
60 (All)	0.007	1.829	0.319	2.490	1.000	0.428	0.0985
Unpol	0.015	1.7	0.2	1.8	1.2	0.2	

PNT 66 MWIR cross-terms cases do not have errors as low as the $ss - ss$ or $pp - pp$ cases in Table 20. The lowest error case, $pp - ss$ has an error that is a little less than twice as much of $ss - ss$ or $pp - pp$. This is shown in Figure 14(b), where the 30° matches well for a large range of scattered angles. The 60° case matches well for scattered angles starting at around 10°. The parameters on unpolarized data have

36
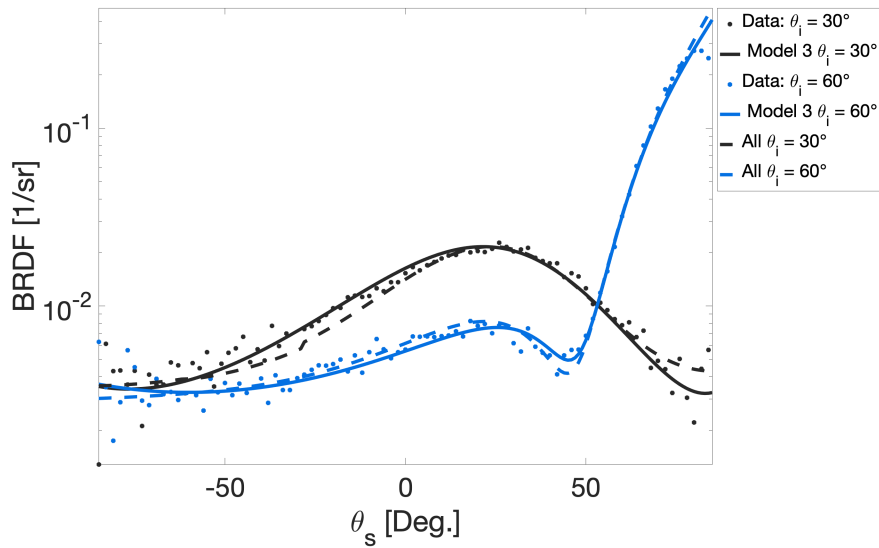
(a) PNT 66 MWIR pp polarization
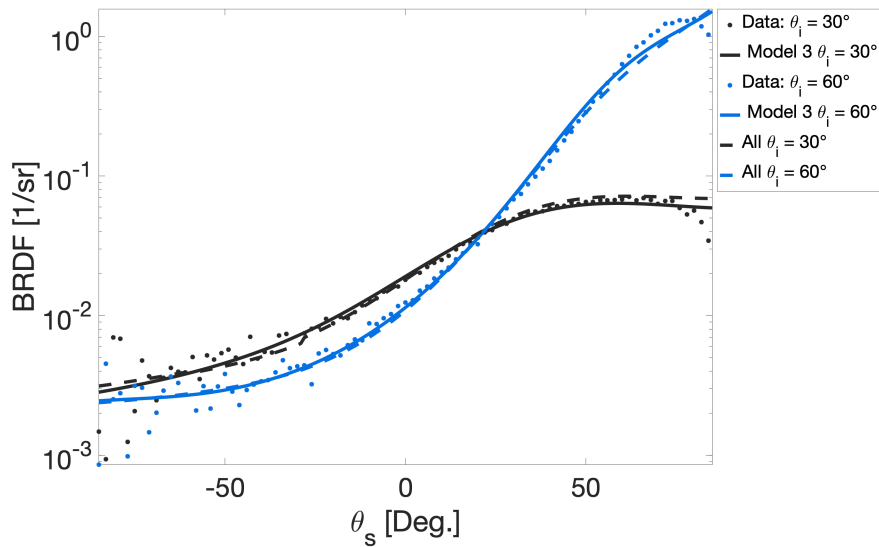
(b) PNT 66 MWIR ss polarization

Figure 13. PNT 66 MWIR pp and ss polarization have accurate fits except in the backscatter and grazing angles. The model optimized at each incident angle and parameters fitted to all of the data fit the data comparably well.

twice as much error as the $pp - ss$ case, but seem to match the data at scattered angles around $0°$ as shown in Figure 14(c) and 14(d).

In the NIR case, the error terms are nearly an order of magnitude smaller than the

37
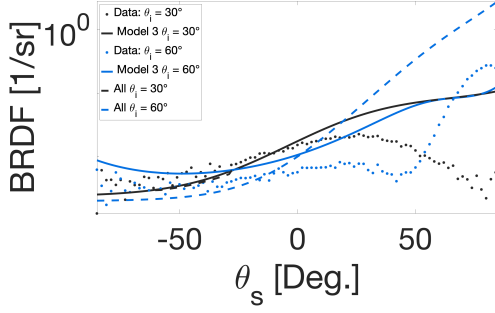
(a) PNT 66 MWIR ss on pp data
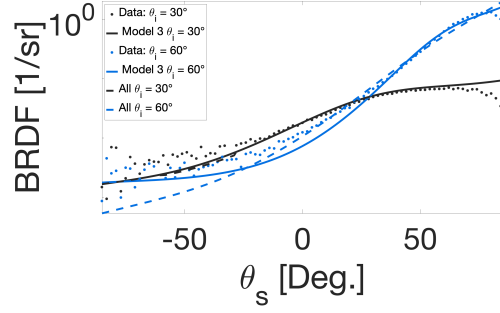
(b) PNT 66 MWIR pp on ss data
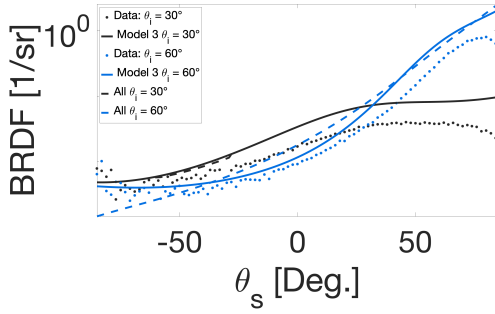
(c) PNT 66 MWIR pp on unpolarized data
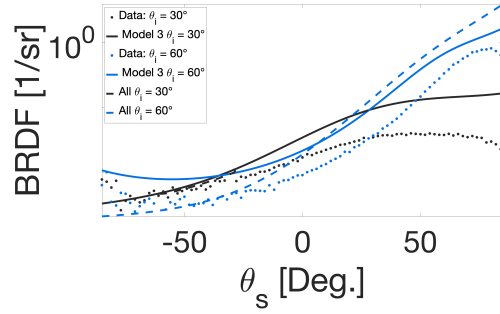
(d) PNT 66 MWIR ss on unpolarized data

Figure 14. PNT 66 MWIR cross term cases have the lowest error for the pp paramters on ss polarization data case

Table 20. PNT 66 MWIR polarization term error is lowest in the cross-term sense for $pp - ss$ **for four of four cases and** $pp - unp$ **for three of four cases.**

θ	ss-ss	ss-pp	ss-unp	pp-pp	pp-ss	pp-unp
30	0.0175	0.1093	0.0688	0.0169	0.0294	0.0507
30 (All)	0.0959	0.1162	0.0756	0.1147	0.0902	0.0868
60	0.0188	0.0812	0.0659	0.0145	0.0307	0.0369
60 (All)	0.0985	0.2383	0.1623	0.1248	0.1220	0.1323

MWIR PNT 66 case, shown in Tables 23 and 20. For both of the $60°$ cases in both the ss and pp polarization cases, the n and κ terms, respectively, are not physically realistic in Tables 22 and 21. The ss polarization case terms are around half those in the pp polarization case. The pp case has more curves, as can be seen in Figure 15(a), which would contribute to this difference in error. Despite this, the error terms are

38

relatively low, meaning that the parameters do fit the data, even though there are some terms that are not physically realistic.

(a) PNT 66 NIR pp polarization
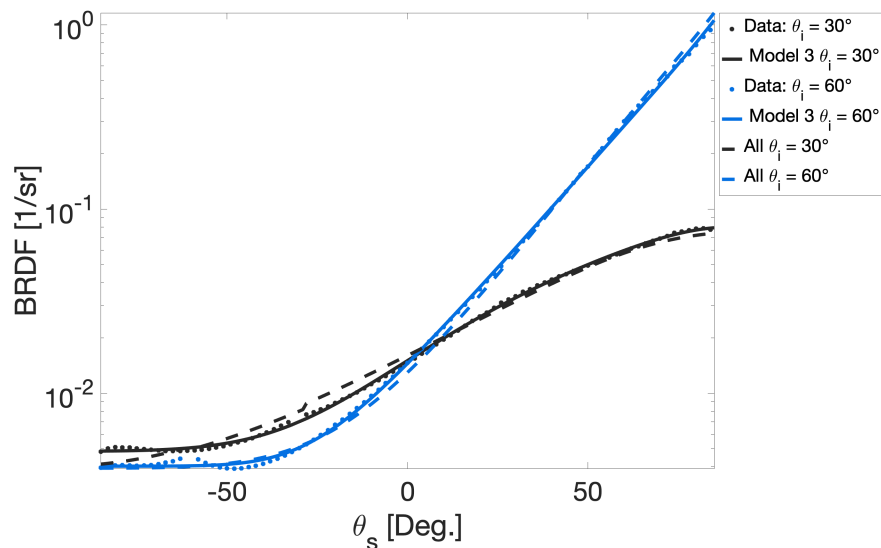
(b) PNT 66 NIR ss polarization

Figure 15. PNT 66 NIR ss polarization has lower error than pp due to the backscatter

PNT 66 NIR cross-terms again are the best for *pp* parameters on *ss* polarized data in Table 23. Figure 16(b) shows that this is true for 30° at angles around 0°. Figure

Table 21. PNT 66 NIR pp parameters are consistent with unpolarized parameters for ρ_d, ρ_s, s, and n. κ is at its minimum bound of 0 for the 'all' parameters, which may be problematic.

θ(deg)	ρ_d	ρ_s	s	q	n	κ	Log. Error
30	0.001	3.271	0.401	2.715	1.390	0.033	0.0045
30 (All)	0.011	1.626	0.346	2.884	1.394	0.000	0.0937
60	0.013	1.234	0.539	5.293	1.385	0.000	0.0041
60 (All)	0.011	1.626	0.346	2.884	1.394	0.000	0.1044
Unpol	0.015	1.7	0.3	2.1	1.2	0.2	

Table 22. PNT 66 NIR ss parameters are consistent with unpolarized parameters for ρ_d. n is bottomed out in the 'all' parameters and $60°$ case, which may mean the ss Rayleigh-Rice term is problematic.

θ(deg)	ρ_d	ρ_s	s	q	n	κ	Log. Error
30	0.015	5.048	0.696	8.692	1.122	0.148	0.0018
30 (All)	0.012	1.532	0.643	5.327	1.000	0.413	0.0769
60	0.013	1.272	0.951	10.000	1.000	0.499	0.0025
60 (All)	0.014	0.223	0.698	5.247	1.000	2.558	0.0758
Unpol	0.015	1.7	0.3	2.1	1.2	0.2	

16(c) and 16(d) show that when modeled on unpolarized data, the model matches the data well only at select angles. On unpolarized data, pp parameters model $60°$ reasonably well past scattered angles of $10°$. For ss parameters on unpolarized data, the entire backscatter area for both incident angles are modeled fairly well. No cross term case performs well enough to compare to the $ss - ss$ or $pp - pp$ terms as they are all an order of magnitude higher in error than those cases.

For PNT 66, the UV case does have a similar shape to the NIR case, but with a higher backscatter term, shown in Figure 17. As in the previous cases, there are erroneous terms in the indices of refraction: three out of the four cases have either κ as 0 or the real part of the index of refraction as 1 in Table 25. Also of note are that both the ρ_d terms in the pp polarization case are 0 in Table 24. The pp

40
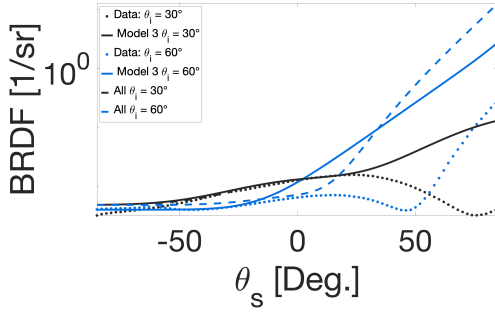
(a) PNT 66 NIR ss on pp data
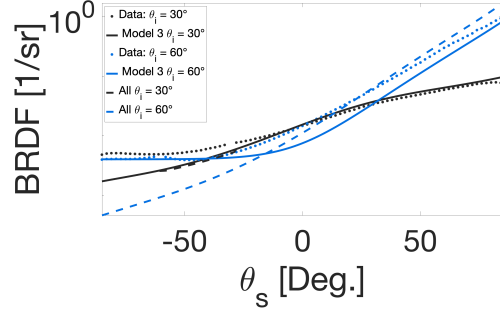
(b) PNT 66 NIR pp on ss data
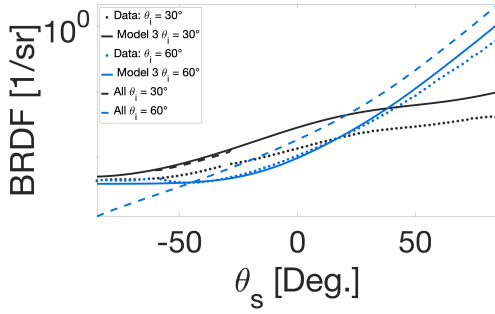
(c) PNT 66 NIR pp on unpolarized data
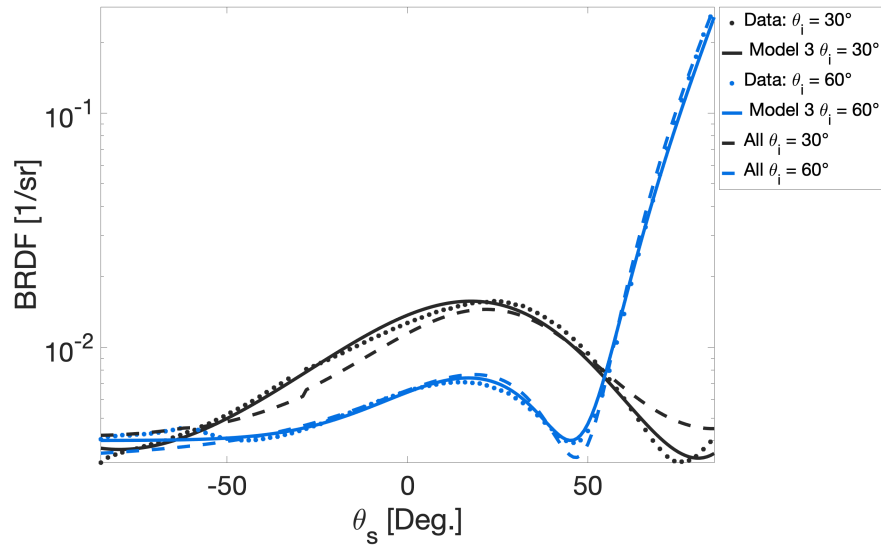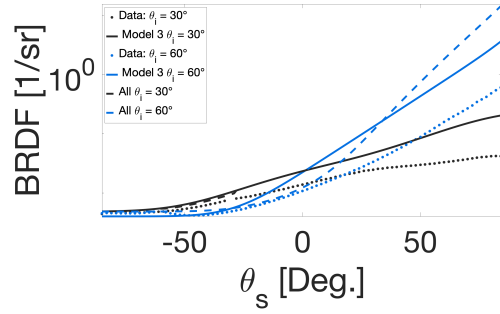

(d) PNT 66 NIR ss on unpolarized data

Figure 16. PNT 66 NIR has the lowest error in fitting either ss or pp parameters on unpolarized data for the lower and higher incident angle, respectively

Table 23. PNT 66 NIR polarization term error shows that pp parameters better model cross term data than ss parameters. $pp - ss$ has a lower error for four of four cases, and $pp - unp$ has a lower error for three of four cases.

θ	ss-ss	ss-pp	ss-unp	pp-pp	pp-ss	pp-unp
30	0.0018	0.1047	0.0582	0.0045	0.0304	0.0486
30 (All)	0.0769	0.1103	0.0582	0.0937	0.0716	0.0655
60	0.0025	0.1535	0.0808	0.0041	0.0317	0.0156
60 (All)	0.0758	0.3003	0.2086	0.1044	0.1277	0.1299

polarization case is also interesting since the higher incident angle term has a lower logarithmic error than the lower incident angle case. Similarly, the ρ_d term in the 30° ss polarization case is 0, but in this case the error is lower than the higher incident term, which is what is normally expected.

41

Table 24. PNT 66 UV pp parameters match well for s and q with unpolarized parameters. The indices of refraction are also consistent between the three sets of parameters at a value other than 1, unlike in Table 25.

θ(deg)	ρ_d	ρ_s	s	q	n	κ	Log. Error
30	0.000	3.565	0.411	2.651	1.397	0.000	0.0053
30 (All)	0.008	1.989	0.287	2.014	1.411	0.000	0.0808
60	0.000	2.770	0.333	1.838	1.427	0.056	0.0030
60 (All)	0.008	1.989	0.287	2.014	1.411	0.000	0.0973
Unpol	0.015	1.7	0.3	2.2	1.2	0.2	

Table 25. PNT 66 UV ss parameters agree exactly with unpolarized ρ_d parameter. The 'all' parameters hit the upper bound for q and the lower bound for n, which indicate difficulties in optimizing the parameter values.

θ(deg)	ρ_d	ρ_s	s	q	n	κ	Log. Error
30	0.000	4.292	0.368	1.759	1.467	0.000	0.0030
30 (All)	0.015	1.317	0.984	10.000	1.000	0.473	0.0700
60	0.015	0.605	0.773	7.381	1.000	0.967	0.0038
60 (All)	0.015	1.317	0.984	10.000	1.000	0.473	0.0656
Unpol	0.015	1.7	0.3	2.2	1.2	0.2	
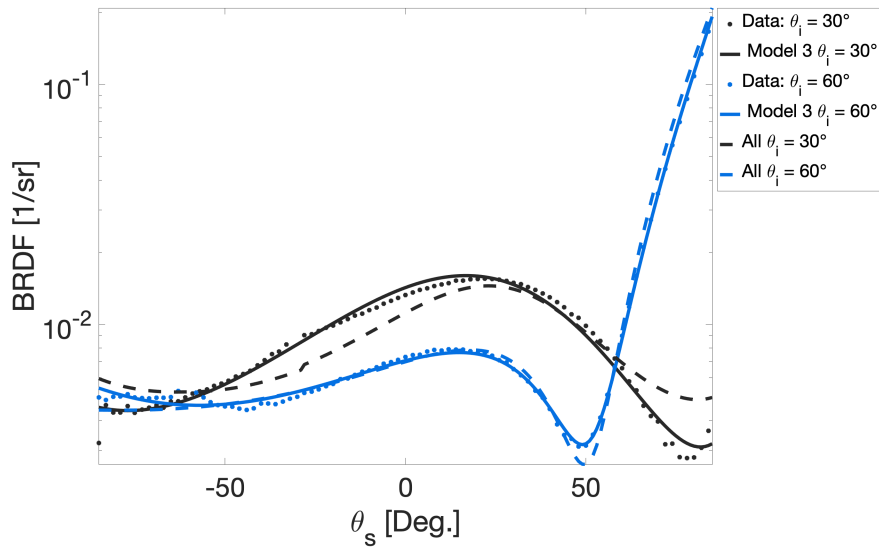
(a) PNT 66 UV pp polarization
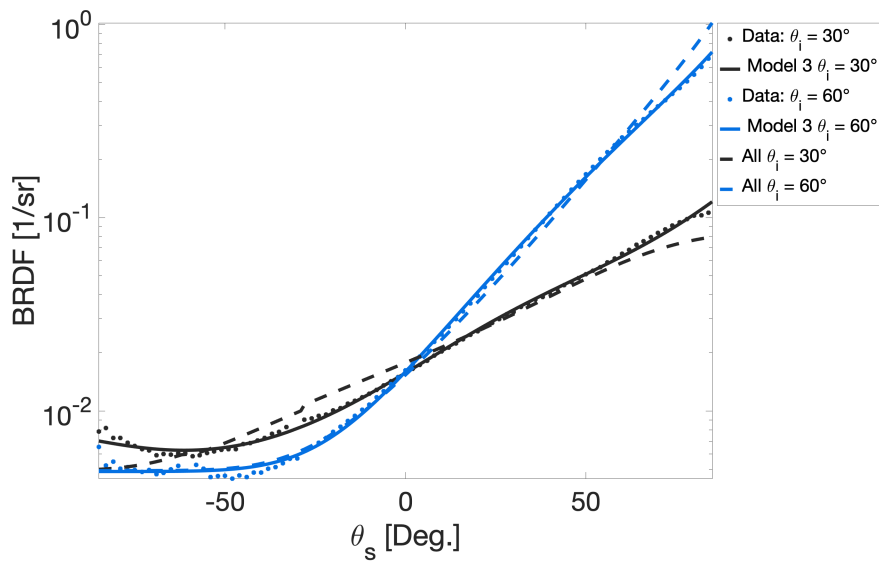
(b) PNT 66 UV ss polarization

Figure 17. PNT 66 UV pp polarization data is well modeled by both sets of parameters. Unlike in other cases, the model and the model using the 'all' parameters performs comparably well, but struggle at the grazing angle.

PNT 66 UV cross-term cases do not perform as well or comparably to $ss - ss$ or $pp - pp$ cases, but the $pp - ss$ case does have the lowest error in Table 26. Although

43

the error for this case is still an order of magnitude larger than the $ss - ss$ or $pp - pp$ cases, Figure 18(b) shows that there are some portions of scattered angles that the model accurately fits to the ss polarization data. Most of the other cross-term cases perform on the same level of magnitude of error, but the ss parameters on pp data has the highest value of error in the $60°$ case.
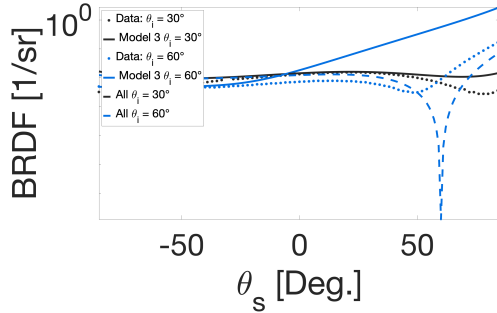
(a) PNT 66 UV ss on pp data
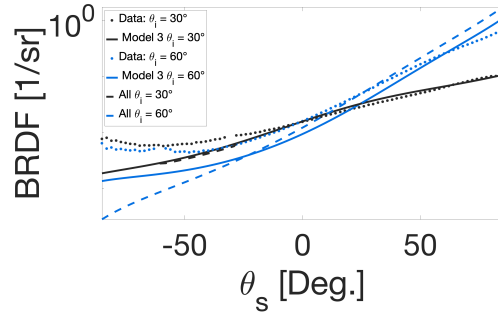
(b) PNT 66 UV pp on ss data
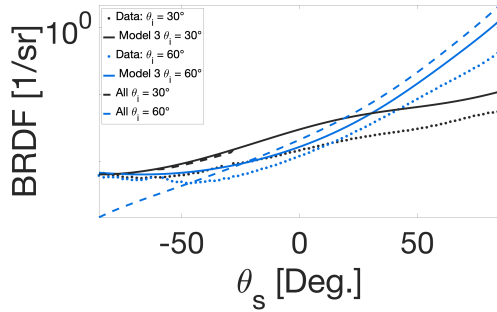
(c) PNT 66 UV pp on unpolarized data
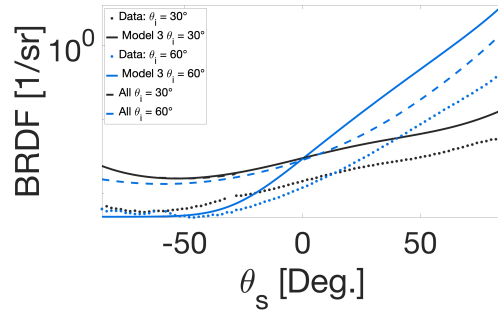
(d) PNT 66 UV ss on unpolarized data

Figure 18. PNT 66 UV has the lowest crossterm error for pp parameters on ss polarization data

Table 26. PNT 66 UV polarization term error is better in three of four cases for both *pp − ss* **and** *pp − unp* **than** *ss − pp* **and** *ss − unp*.

θ	ss-ss	ss-pp	ss-unp	pp-pp	pp-ss	pp-unp
30	0.0030	0.0496	0.0643	0.0053	0.0364	0.0468
30 (All)	0.0700	0.0774	0.0869	0.0808	0.0653	0.0595
60	0.0038	0.1758	0.0915	0.0030	0.0488	0.0372
60 (All)	0.0656	0.1423	0.1265	0.0973	0.1431	0.1300

4.4   PNT 36375 NIR

For PNT 36375 NIR, the *pp* and *ss* polarization seem to perform comparably, with the *ss* polarization case performing slightly better overall. While these data sets clearly have a backscatter peak for each case, the model does not attempt to fit to those data points in Figure 19. For all of the *ss* cases in Table 31, the index of refraction, n, is 1, while in the 20° and 40° case, κ is at its maximum value of 100. For those incident angles, q is also at its maximum value of 10, while the rest of the parameters are parameters that seem reasonable. Again, there is a diffuse fitting parameter, ρ_d of 0 for the 60° case in the *ss* polarization, but this case also has the lowest logarithmic error. In addition, the specular fitting parameter for the 80° case seems unreasonably large at approximately 197. For all of the initial guess iterations mentioned in the methodology, this specular fitting parameter was around 197 for the cases with the lowest logarithmic error. Also, this is in the case of a high incident angle, which may contribute to the parameters being less reliable; in both *pp* and *ss* cases the highest incident angle cases have the highest logarithmic errors, seen in Tables 27 and 28. The microfacet model may not be appropriate for high incident angles in general, so more work would need to be done for those scattered angles. Another interesting parameter result was that of ρ_s as 0 for the *pp* polarization 40° incident angle case. Not only does this case have this, but also the other parameters

45

are either at their upper or lower bound. According to the equation of this model, if ρ_s is 0, the rest of the equation is 0, except for the diffuse term which in this case has a non-zero value. Based on this, and the high index of refraction of approximately 99, this fit may have been at the global minimum for MATLAB®'s lsqcurvefit, but the values do not seem realistic in any way.

Table 27. PNT 36375 NIR pp parameters do not follow a consistent trend. In many cases, q, n, and κ reach their maximum or minimum value. The 'all' parameter κ matches well with the unpolarized κ.

θ(deg)	ρ_d	ρ_s	s	q	n	κ	Log. Error
20	0.156	11.467	1.155	10.000	1.306	0.000	0.0036
20 (All)	0.208	0.405	0.962	1.500	1.000	0.022	0.0924
40	0.218	0.000	10.000	1.500	99.893	0.000	0.0067
40 (All)	0.208	0.405	0.962	1.500	1.000	0.022	0.0873
60	0.125	6.364	3.066	10.000	1.675	0.210	0.0037
60 (All)	0.208	0.405	0.962	1.500	1.000	0.022	0.0770
80	0.169	0.538	1.957	2.573	1.000	0.014	0.0081
80 (All)	0.208	0.405	0.962	1.500	1.000	0.022	0.1385
Unpol	0.35	1.7	0.3	1.5	1.2	0.2	

Table 28. PNT 36375 NIR ss parameters vary quite significantly. The highest incident angle has a ρ_s an order of magnitude higher than all of the others. Also of note is that for parameters q, n, and κ, the maximum or minimum bound is reached in the majority of cases.

θ(deg)	ρ_d	ρ_s	s	q	n	κ	Log. Error
20	0.176	0.309	1.649	10.000	1.000	100.000	0.0044
20 (All)	0.231	5.614	0.207	1.500	1.128	0.000	0.1072
40	0.127	1.257	2.633	10.000	1.000	100.000	0.0045
40 (All)	0.231	5.614	0.207	1.500	1.128	0.000	0.0934
60	0.000	7.725	2.051	3.262	1.000	1.849	0.0038
60 (All)	0.231	5.614	0.207	1.500	1.128	0.000	0.0769
80	0.123	197.035	0.873	1.654	1.000	0.032	0.0057
80 (All)	0.231	5.614	0.207	1.500	1.128	0.000	0.1387
Unpol	0.35	1.7	0.3	1.5	1.2	0.2	

PNT 36375 NIR is modeled best in the $ss-ss$ and $pp-pp$ cases, shown in Table 29.

46
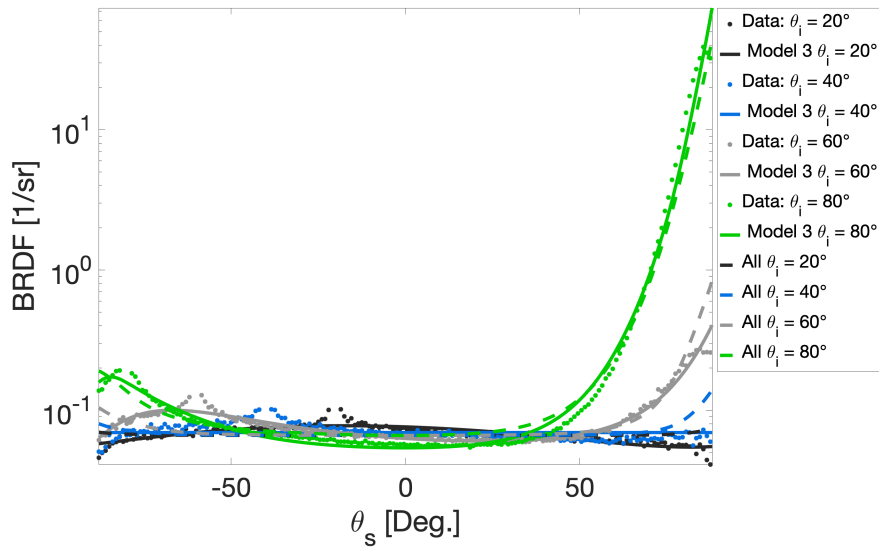
(a) 36375 NIR pp polarization
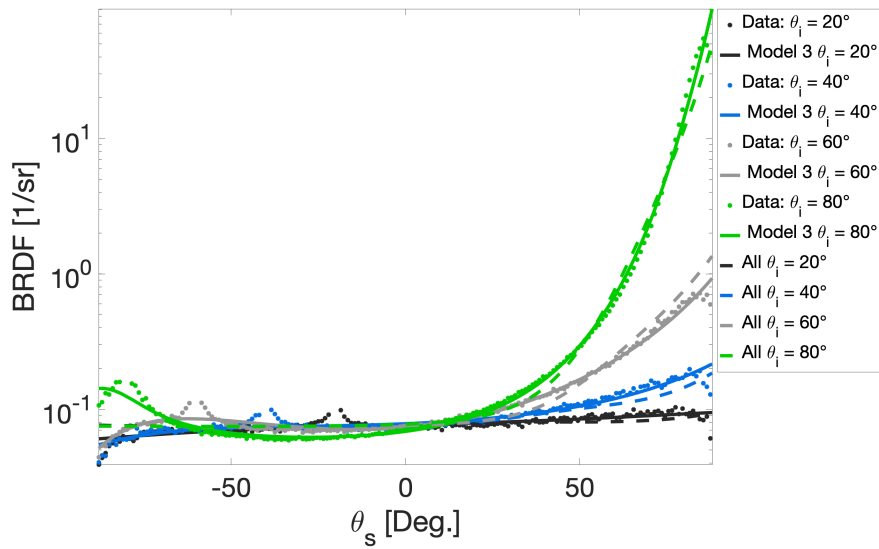
(b) 36375 NIR ss polarization

Figure 19. PNT 36375 NIR have very visible backscatter peaks. Despite this, the rest of the fits seem to model the data well in both polarizations and both parameter approaches.

When using cross-terms, *pp* parameters model *ss* polarization better than parameters on any other set of data. The *ss* parameters notably do not perform well on other sets of data, as can be seen in Figures 20(a) and 20(d) with the model struggling

47

at high incident angles. On the other hand Figures 20(b) and 20(c) show that *pp* parameters model *ss* polarization and unpolarized data relatively similarly.

(a) 36375 NIR ss on pp data

(b) 36375 NIR pp on ss data

(c) 36375 NIR pp on unpolarized data

(d) 36375 NIR ss on unpolarized data
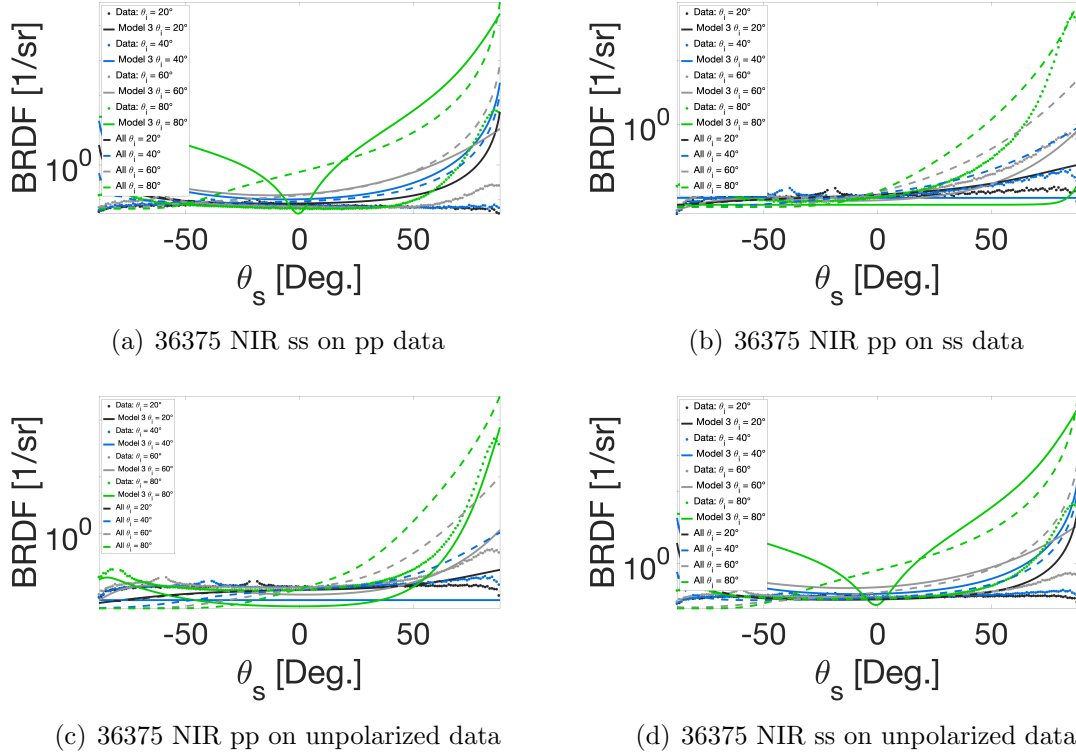
Figure 20. PNT 35375 NIR pp parameters on ss polarization data has the lowest error of majority of crossterm cases

Table 29. PNT 36375 NIR polarization term error shows that *pp* parameters model data in all cases than *ss* data.

θ	ss-ss	ss-pp	ss-unp	pp-pp	pp-ss	pp-unp
20	0.0044	0.0772	0.0601	0.0036	0.0172	0.0160
20 (All)	0.1072	0.1203	0.0915	0.0924	0.0872	0.0806
40	0.0045	0.1186	0.0956	0.0067	0.0207	0.0334
40 (All)	0.0934	0.1464	0.1140	0.0873	0.0763	0.0692
60	0.0038	0.0930	0.0713	0.0037	0.0139	0.0131
60 (All)	0.0769	0.2192	0.1799	0.0770	0.1059	0.1221
80	0.0057	0.2327	0.2067	0.0081	0.1088	0.0315
80 (All)	0.1387	0.4138	0.3627	0.1385	0.1878	0.2249

48

4.5 PNT 36495 VIS

In the visible spectrum, PNT 36495 performs comparably with other materials, but the high incident of angle of 85° creates more error, shown in Tables 31 and 30. Although there are backscatter peaks in these plots, the model only attempts to fit the data in the pp polarization case, shown in Figure 21. As with most other materials there are problematic cases where n is 1 and κ is 0. Due to the strong backscatter peak in the 85° case, the logarithmic error in this case is about twice as much as the other incident angle cases. Since this material is highly diffuse, the data is mostly flat. An interesting comparison between the pp and ss data is that all of the cases have comparable ρ_d values between 0.220 to 0.260, which was only seen in a few of the materials.

Table 30. PNT 36495 VIS pp parameters hit the lower bound often for q and n, however the q lower bound matches the unpolarized q parameter. ρ_d and κ are consistent between the sets of parameters.

θ(deg)	ρ_d	ρ_s	s	q	n	κ	Log. Error
30	0.259	6.394	0.693	4.971	1.382	0.000	0.0051
30 (All)	0.283	0.725	1.179	1.500	1.000	0.069	0.1178
60	0.250	3.602	3.011	10.000	1.548	0.312	0.0062
60 (All)	0.283	0.725	1.179	1.500	1.000	0.069	0.0973
85	0.235	1.037	1.403	1.500	1.000	0.068	0.0104
85 (All)	0.283	0.725	1.179	1.500	1.000	0.069	0.1507
Unpol	0.5	1.7	0.2	1.5	1.2	0.2	

**Table 31. PNT 36495 VIS ss parameters hit the lower bound of n in the 'all' and 30°
case. No parameters match well with the unpolarized parameters.**

$\theta(\text{deg})$	ρ_d	ρ_s	s	q	n	κ	Log. Error
30	0.223	0.756	0.847	4.522	1.000	1.989	0.0051
30 (All)	0.248	1.087	0.455	3.062	1.000	0.833	0.1323
60	0.260	0.745	0.247	2.133	1.130	0.913	0.0065
60 (All)	0.248	1.087	0.455	3.062	1.000	0.833	0.0869
85	0.251	1.159	0.995	10.000	2.140	0.016	0.0144
85 (All)	0.248	1.087	0.455	3.062	1.000	0.833	0.1405
Unpol	0.5	1.7	0.2	1.5	1.2	0.2	

PNT 36495 VIS has the best fits for $ss - ss$ and $pp - pp$ compared to the other
cross-term cases, shown in Table 32. For the lower incident angles the pp parameters
on ss polarization data had the lowest error. The 85° incident angle was best fit in
the cross-term cases with the ss parameters on unpolarized data. This is best seen
in Figure 22(d), but the model never gets close enough to the data to properly model
it.
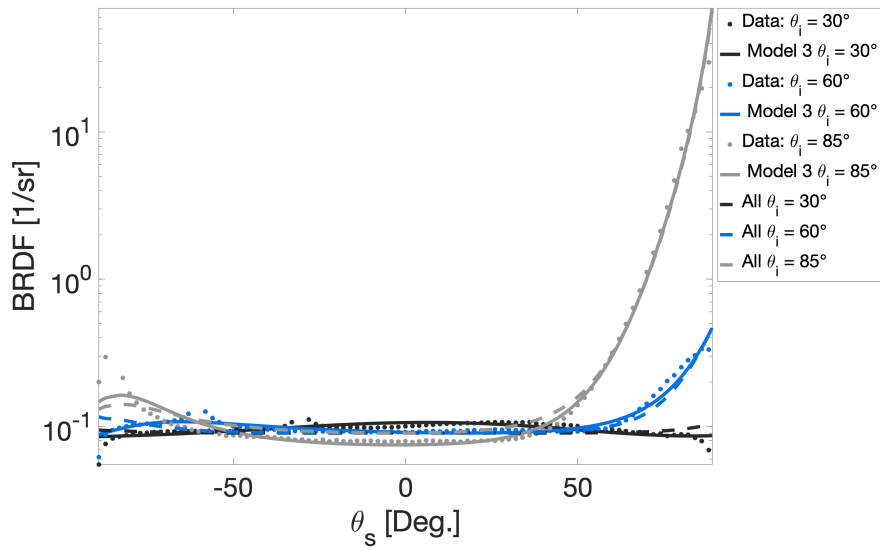
(a) 36495 VIS pp polarization
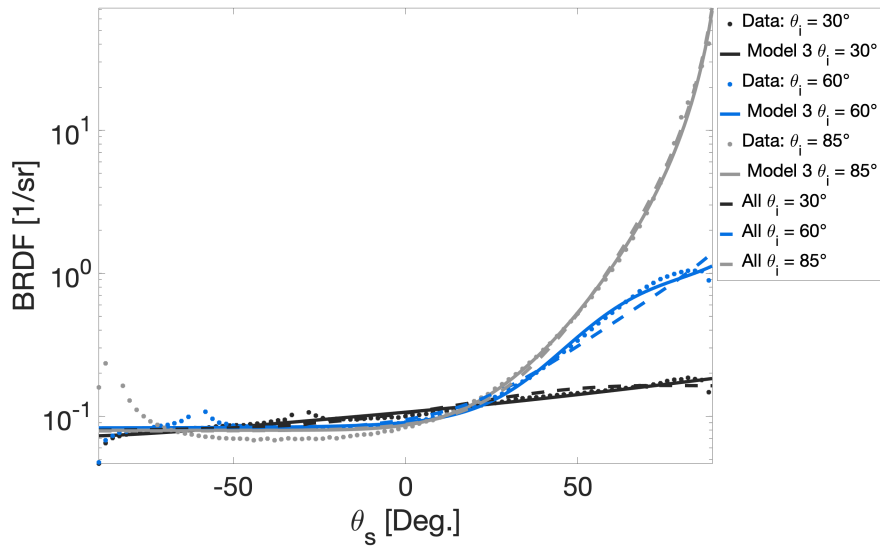
(b) 36495 VIS ss polarization

Figure 21. PNT 36495 VIS shows visible backscatter peaks in both the pp and ss polarization. The model attempts to model the backscatter peaks in the pp polarization, but less so in the ss polarization.

51

Table 32. PNT 36495 VIS polarization term error, where $pp - ss$ **has lower error than** $ss - pp$ **in four of six cases, while** $pp - unp$ **has lower error than** $ss - unp$ **in five of six cases.**

θ	ss-ss	ss-pp	ss-unp	pp-pp	pp-ss	pp-unp
30	0.0051	0.0606	0.0439	0.0051	0.0158	0.0290
30 (All)	0.1323	0.0900	0.0800	0.1178	0.1152	0.1060
60	0.0065	0.0915	0.0683	0.0062	0.0480	0.0405
60 (All)	0.0869	0.1711	0.1309	0.0973	0.0916	0.0962
85	0.0144	0.0745	0.0672	0.0104	0.1242	0.0498
85 (All)	0.1405	0.3333	0.2808	0.1507	0.2034	0.2388
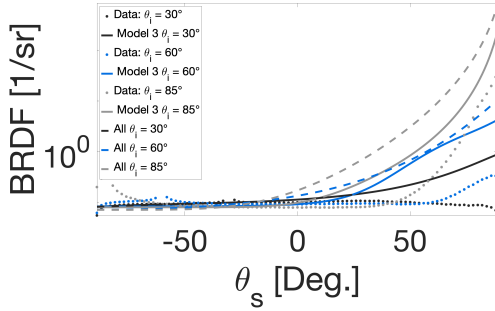
(a) 36495 VIS ss on pp data
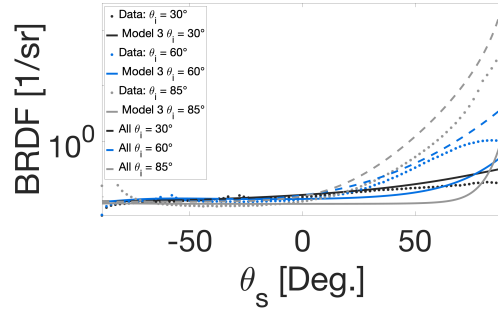
(b) 36495 VIS pp on ss data
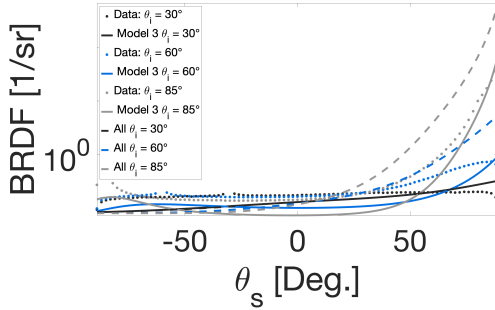
(c) 36495 VIS pp on unpolarized data
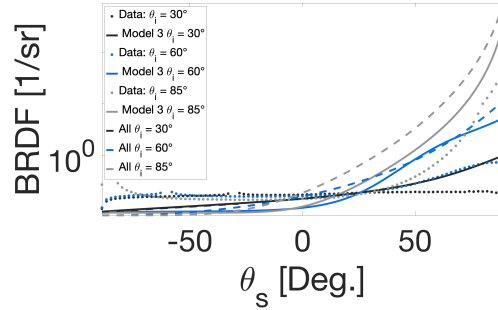
(d) 36495 VIS ss on unpolarized data

Figure 22. PNT 36495 NIR pp parameters fitted onto ss polarization data has lowest error for majority of incident angles

4.6 STD 00696 MWIR

For the NIST standard material, STD 00696, five different incident angles worth of data were taken, shown in Tables 34 and 33, and 23. Between the ss and pp polarization cases the logarithmic error is somewhat similar despite the fitted parameters being quite varied. In the pp polarization case the ρ_s values increase with increasing incident angle, while in the ss polarization case, this parameter varies between the incident angles. The index of refraction terms are of concern in all but one of the pp polarization incident angles, and three of the five cases in the ss polarization. Also of interest is the ρ_d as 0 for the 20 ° in the ss polarization case while all other values for this parameter are non-zero. In the figure, the model seems to fit each data line well. Some backscatter data can be seen, but since it varies so much, contributes to the overall error of the fit.
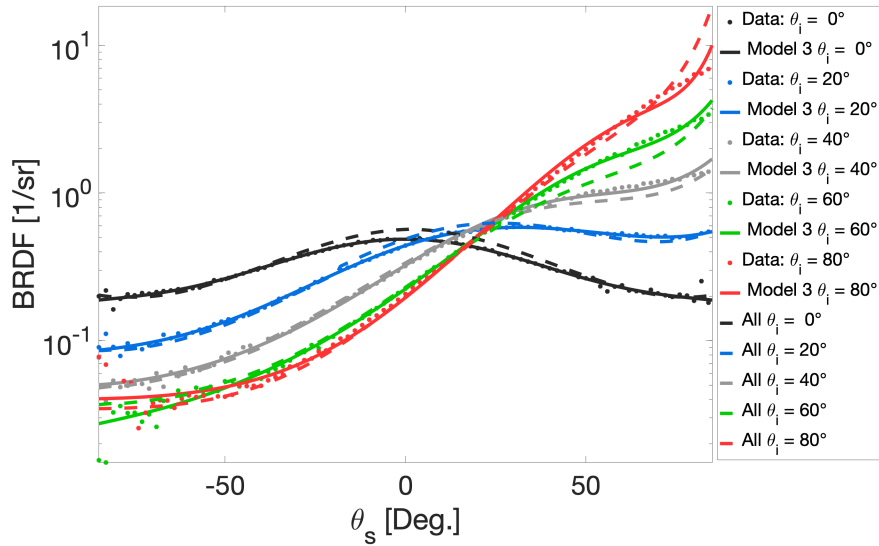
(a) STD 00696 MWIR pp polarization
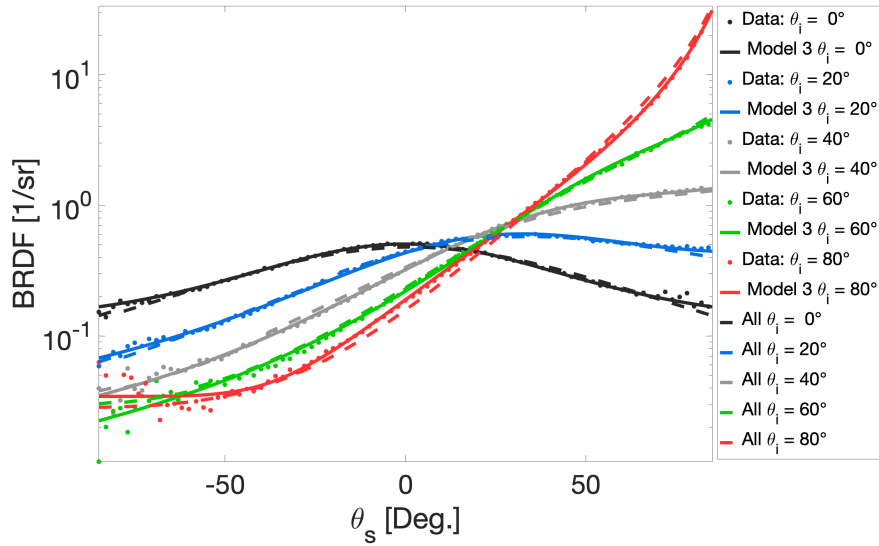
(b) STD 00696 MWIR ss polarization

Figure 23. STD 00696 MWIR ss and pp polarization fits have comparable fits, for both the model with each incident angle parameters and the 'all' parameters. The backscatter data and grazing angle data is not well modeled.

For STD 00696, the 0° case does not follow the trend of many other materials as $ss - pp$ has error that is very comparable to the $ss - ss$ and $pp - pp$ cases. In

54

Table 33. STD 00696 MWIR pp parameters don't match well with their corresponding unpolarized parameter. ρ_s, s, q, and n stay consistent throughout each incident angle and the 'all' parameters. κ is consistently 0, which hits the lower bound.

θ(deg)	ρ_d	ρ_s	s	q	n	κ	Log. Error
0	0.530	0.839	0.569	8.350	1.000	4.609	0.0029
0 (All)	0.108	32.243	0.421	3.302	1.679	0.000	0.2159
20	0.220	18.747	0.506	4.544	1.722	0.326	0.0025
20 (All)	0.108	32.243	0.421	3.302	1.679	0.000	0.1395
40	0.088	29.953	0.376	2.841	1.721	0.000	0.0054
40 (All)	0.108	32.243	0.421	3.302	1.679	0.000	0.1151
60	0.023	40.533	0.304	2.326	1.674	0.000	0.0090
60 (All)	0.108	32.243	0.421	3.302	1.679	0.000	0.1378
80	0.126	49.050	0.335	3.033	1.643	0.000	0.0104
80 (All)	0.108	32.243	0.421	3.302	1.679	0.000	0.1890
Unpol	0.6	0.5	0.12	3.7	1.8	0.2	

all other incident angle cases of STD 00696, $pp - ss$ has the lowest error. Tables 33 and 34 shows that the error, with the exception of 0° follows the trend that all error values increase with increasing incident angle. This trend can also be seen in Table 35 where, for $pp - ss$, from 20° to 80° the error terms increase by an order of magnitude.

Between the 'all' parameters and the parameters from each of the incident cases, the model fits the data fairly well throughout Figures 24(a), 24(b), 24(c), and 24(d) fairly well at lower incident angles. Each case seems to decrease the goodness of the fit with increasing incident angle. The dashed lines representing the 'all' fits also do not fit the data as consistently well as the model using parameters optimized at each incident angle. The 0° line is consistently modeled the most accurately, probably due to its low variation.

Table 34. STD 00696 MWIR ss parameters are somewhat consistent for ρ_d and ρ_s. n has quite the variation between each incident angle, and the 'all' parameter is higher than in any incident angle case.

$\theta(\textbf{deg})$	ρ_d	ρ_s	$\textbf{s}$	$\textbf{q}$	$\textbf{n}$	κ	**Log. Error**
0	0.402	15.492	0.424	3.862	1.768	0.000	0.0029
0 (All)	0.089	4.287	0.471	2.561	13.781	2.410	0.2362
20	0.000	7.050	0.349	1.719	7.746	0.038	0.0025
20 (All)	0.089	4.287	0.471	2.561	13.781	2.410	0.1605
40	0.061	5.192	0.395	2.099	4.706	4.541	0.0057
40 (All)	0.089	4.287	0.471	2.561	13.781	2.410	0.1295
60	0.042	4.370	0.338	1.719	1.000	100.000	0.0086
60 (All)	0.089	4.287	0.471	2.561	13.781	2.410	0.1594
80	0.108	5.584	0.886	5.160	1.000	1.738	0.0092
80 (All)	0.089	4.287	0.471	2.561	13.781	2.410	0.2266
Unpol	0.6	0.5	0.12	3.7	1.8	0.2	
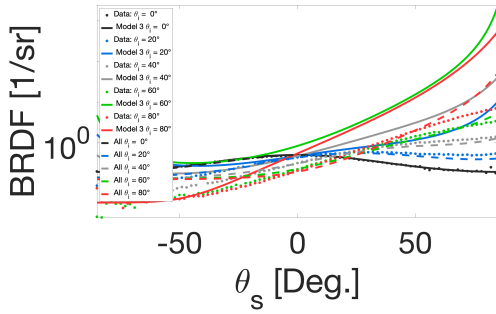
(a) STD00696 ss on pp data
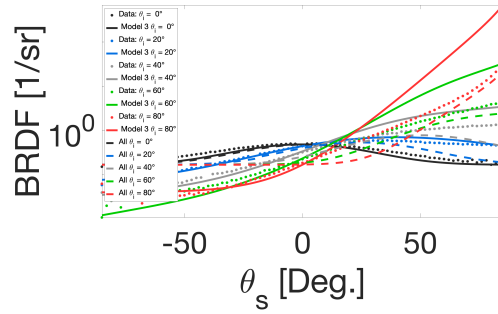
(b) STD00696 pp on ss data
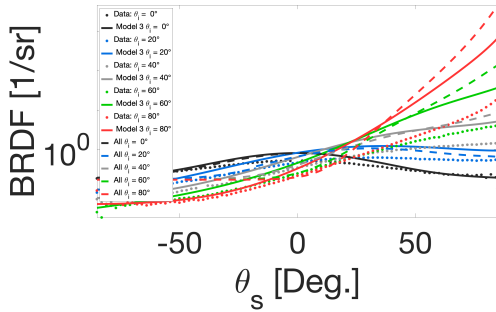
(c) STD00696 pp on unpolarized data
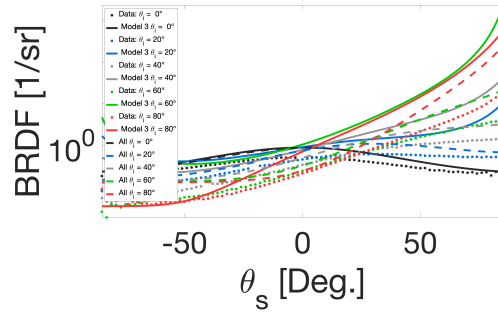
(d) STD00696 ss on unpolarized data

Figure 24. STD 00696 MWIR cross term fits increase in error with incident angle

56

Table 35. STD 00696 MWIR polarization term error is lower in $pp - ss$ for five of 10 cases, while $pp - unp$ is lower in seven of 10 cases.

θ	ss-ss	ss-pp	ss-unp	pp-pp	pp-ss	pp-unp
0	0.0029	0.0032	0.0309	0.0029	0.0119	0.0193
0 (All)	0.2362	0.2135	0.2309	0.2159	0.2355	0.2283
20	0.0025	0.0879	0.1036	0.0025	0.0088	0.0406
20 (All)	0.1605	0.1558	0.1516	0.1395	0.2004	0.1466
40	0.0057	0.0983	0.1097	0.0054	0.0368	0.0579
40 (All)	0.1295	0.1196	0.1304	0.1151	0.1564	0.1674
60	0.0086	0.2001	0.1974	0.0090	0.0737	0.0838
60 (All)	0.1594	0.1228	0.2101	0.1378	0.1300	0.3078
80	0.0092	0.1211	0.1181	0.0104	0.1023	0.1139
80 (All)	0.2266	0.2017	0.3120	0.1890	0.1717	0.4849

4.7   STD 00699 MWIR

For STD 00699 MWIR, ρ_d stays within the same order of magnitude, while ρ_s varies between 2 to over 22, shown in Table 37. The plots are shown in Figure 25. The Hyper-Cauchy parameters s and q vary as well. In one case κ is 0, which is not physically realizable, and two other cases have $n = 0$, another physically problematic case. Between pp and ss, there are only two cases where the fitted ss polarization data is less than the fits to pp polarization data, shown in Table 36. Overall, the fits in both cases tend to increase in error with increasing incident angle.
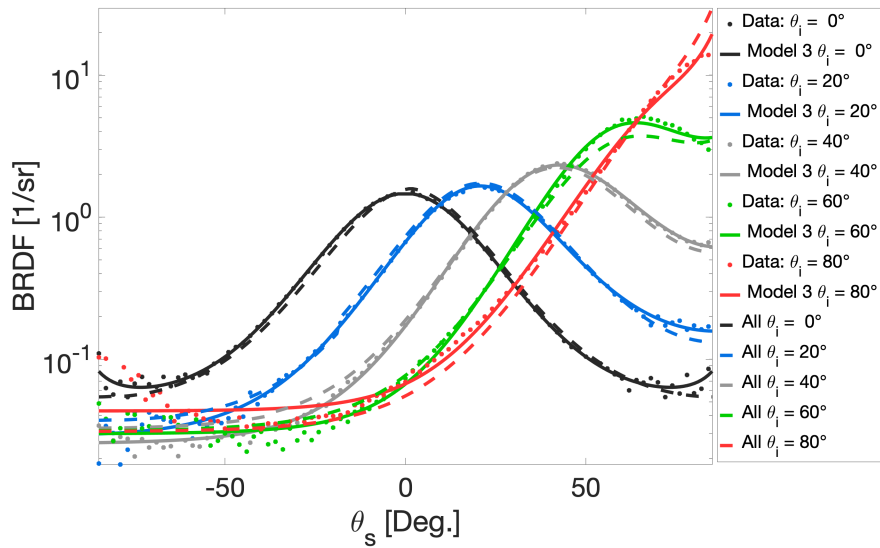
(a) STD 00699 MWIR pp polarization
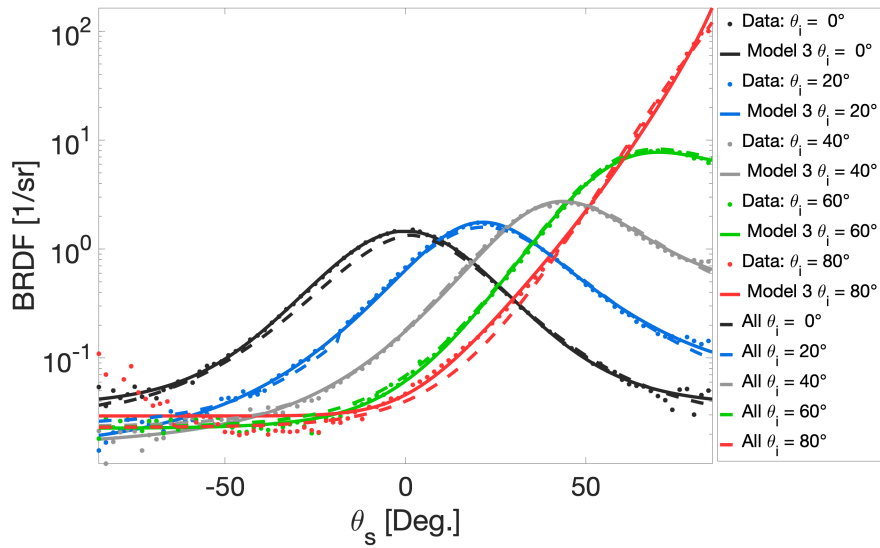
(b) STD 00699 MWIR ss polarization

Figure 25. STD 00699 MWIR fit comparably well between ss and pp polarization, but the backscatter region, especially for higher angles can be seen to not be well-modeled. The 'all' parameters model and the model using the angles optimized for each incident angle seem to compare well.

STD 00699 behaves very similarly to STD 00696. For incident angle 0°, rather

Table 36. STD 00699 MWIR pp parameters compare well with the unpolarized parameters for q and n. The parameters throughout each case stay relatively consistent. κ reaches the lower bound of 0 for all but two cases.

$\theta(\deg)$	ρ_d	ρ_s	s	q	n	κ	Log. Error
0	0.105	2.008	0.229	3.727	10.749	0.001	0.0052
0 (All)	0.098	27.885	0.207	2.697	1.660	0.000	0.3305
20	0.076	59.419	0.193	2.790	1.235	0.289	0.0088
20 (All)	0.098	27.885	0.207	2.697	1.660	0.000	0.2294
40	0.079	24.061	0.217	3.204	1.701	0.013	0.0076
40 (All)	0.098	27.885	0.207	2.697	1.660	0.000	0.1774
60	0.094	32.726	0.209	3.304	1.653	0.000	0.0107
60 (All)	0.098	27.885	0.207	2.697	1.660	0.000	0.2303
80	0.136	38.195	0.225	3.305	1.644	0.000	0.0173
80 (All)	0.098	27.885	0.207	2.697	1.660	0.000	0.2761
Unpol	0.2	0.5	0.15	3.5	1.7	0.2	

Table 37. STD 00699 MWIR ss parameters match fairly well with the unpolarized s parameter. ρ_s is relatively consistent, except at 80° incidence, where the value is over 22.

$\theta(\deg)$	ρ_d	ρ_s	s	q	n	κ	Log. Error
0	0.114	6.894	0.224	3.322	1.000	1.074	0.0056
0 (All)	0.073	3.143	0.197	2.449	7.076	0.011	0.3771
20	0.038	3.596	0.159	1.963	6.661	0.000	0.0077
20 (All)	0.073	3.143	0.197	2.449	7.076	0.011	0.2712
40	0.048	3.524	0.163	1.949	6.393	0.500	0.0089
40 (All)	0.073	3.143	0.197	2.449	7.076	0.011	0.2133
60	0.071	2.773	0.215	2.750	8.139	1.142	0.0103
60 (All)	0.073	3.143	0.197	2.449	7.076	0.011	0.2800
80	0.092	22.860	0.816	8.987	1.000	0.148	0.0229
80 (All)	0.073	3.143	0.197	2.449	7.076	0.011	0.3515
Unpol	0.2	0.5	0.15	3.5	1.7	0.2	

than $ss - pp$ having an error value comparable to $ss - ss$ and $pp - pp$, $ss - unp$ is now the closest in magnitude, shown in Table 38. For the rest of the cases, $pp - ss$ has the smallest error of all the cross-term cases for each incident angle. Figures 26(b) and 26(c) appear to be similar, as the values in Table 38 show, meaning that

59

pp parameters can better be used on *ss* polarization and unpolarized data than *ss* parameters on data other than *ss* polarized.
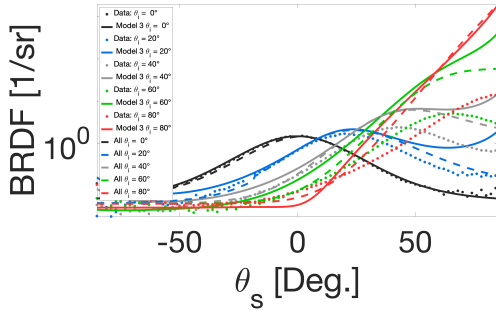
(a) STD00699 ss on pp data
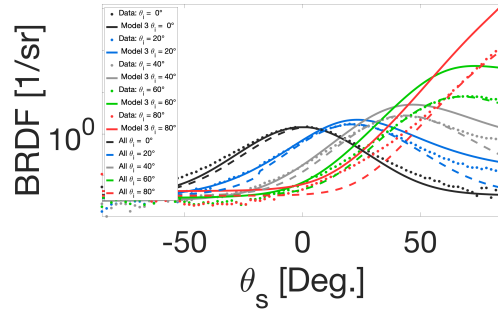
(b) STD00699 pp on ss data
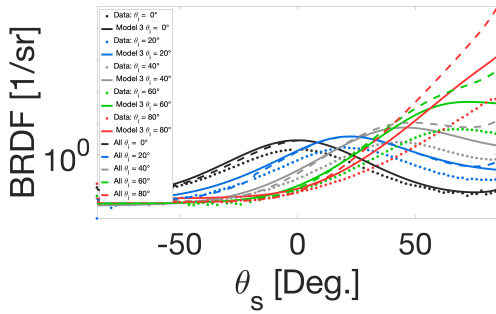
(c) STD00699 pp on unpolarized data
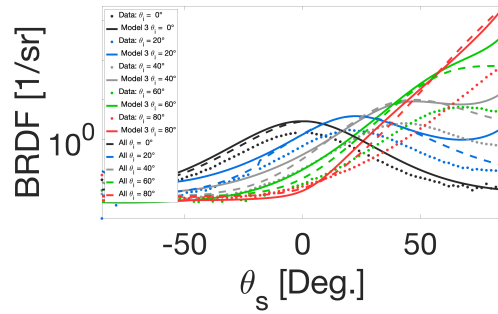
(d) STD00699 ss on unpolarized data

**Figure 26. STD 00699 cross term fit erros increase with increasing incident angle**

Table 38. STD 00699 MWIR polarization term error for seven of the 10 cases, both $pp-ss$ **and** $pp-unp$ **outperform the corresponding cases using ss parameters.**

θ	ss-ss	ss-pp	ss-unp	pp-pp	pp-ss	pp-unp
0	0.0056	0.0110	0.0396	0.0052	0.0201	0.0329
0 (All)	0.3771	0.3302	0.3698	0.3305	0.3895	0.3664
20	0.0077	0.0665	0.0858	0.0088	0.0261	0.0535
20 (All)	0.2712	0.2098	0.2458	0.2294	0.2923	0.2313
40	0.0089	0.0823	0.0928	0.0076	0.0359	0.0579
40 (All)	0.2133	0.2310	0.2533	0.1774	0.2125	0.2785
60	0.0103	0.1281	0.1249	0.0107	0.0676	0.0833
60 (All)	0.2800	0.3786	0.3909	0.2303	0.2828	0.4512
80	0.0229	0.1367	0.1168	0.0173	0.0855	0.0999
80 (All)	0.3515	0.4922	0.4945	0.2761	0.3530	0.6333

4.8   PNT 01006 NIR

PNT 01006 NIR is clearly a specular material as seen from the plots with a high specular peak with high BRDF values at the scattered angle corresponding to the incident angles. Overall, the pp polarization has a lower logarithmic error than the ss polarization cases. Also, the κ value for all of the pp polarization cases is 0, while for all of the ss polarization cases, κ is 100, shown in Tables 40 and 39. As with every case before, the highest incident angle will have the highest error. Also of note is the high index of refraction for the $20°$ case for ss polarization, while all the rest of the cases have an index of refraction around 1. Since the material is the same for all cases, this large range of indices of refraction is never physically accurate. In the pp polarization case, the specular term is large for the two lowest incident angles at around 16 and 27, while the highest incident angle has a ρ_s of 0.370, shown in Table 39 and Figure 27. The error terms for this material are also an order of magnitude larger than the more diffuse materials.

While $ss - ss$ and $pp - pp$ result in the lowest error, the $20°$ case has comparable error for $ss - pp$ and $pp - ss$ terms in Table 41. As the incident angle increases, this

61
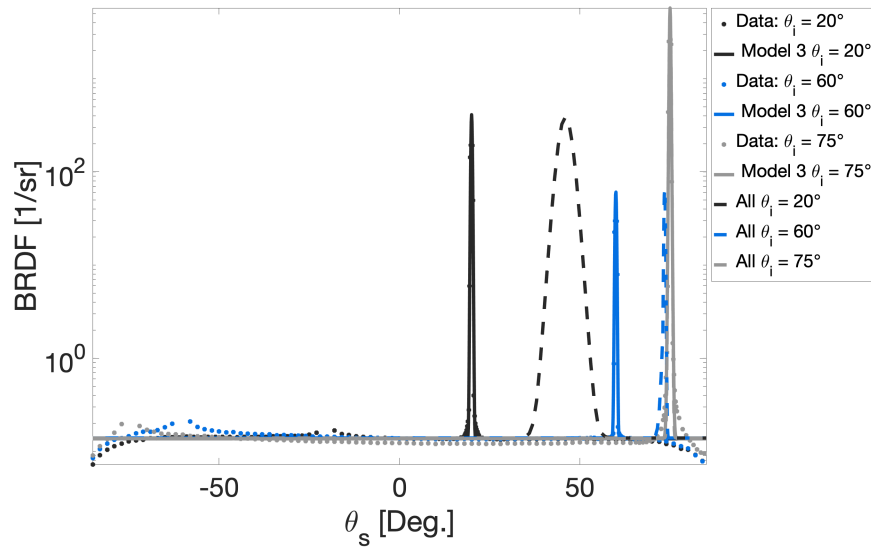
(a) PNT 1006 NIR pp polarization
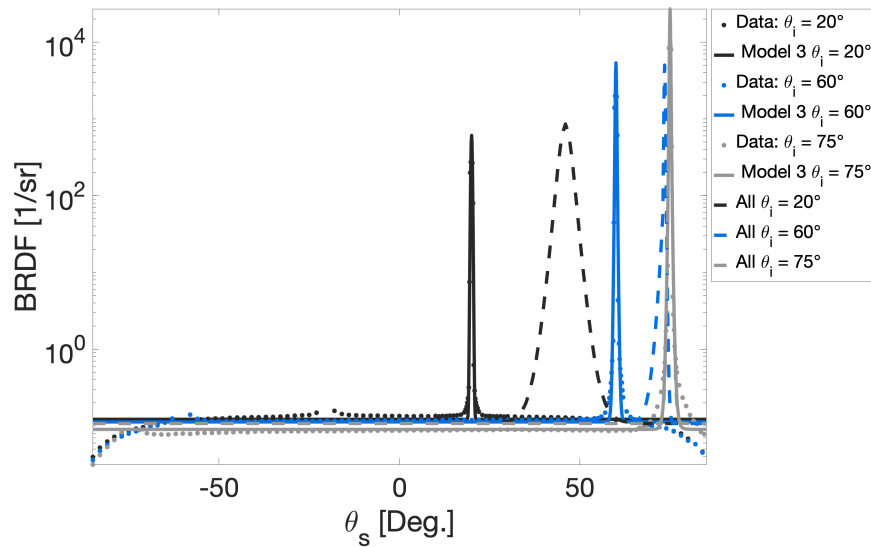
(b) PNT 1006 NIR ss polarization

Figure 27. PNT 1006 NIR data is well-fitted by the model with parameters optimized at each incident angle. The 'all' parameters used with the model, shown in dashed lines, do not properly model any of the peaks.

trend does not hold, but $pp - ss$ tends to be the cross-term case with the lowest error value. For 75° the $ss - pp$ and $ss - unp$ are nearly a whole order of magnitude larger than the error in the 20° case. Figures 28(a) and 28(d) support this as in the 75°

62

Table 39. PNT 01006 NIR pp parameters are consistent for ρ_d, s, q, n, and κ. The n and κ terms do not correspond directly to the unpolarized parameters.

θ(deg)	ρ_d	ρ_s	s	q	n	κ	Log. Error
20	0.429	16.354	0.005	9.997	1.166	0.000	0.0189
20 (All)	0.437	1.182	0.004	9.047	1.489	0.032	0.1958
60	0.438	27.178	0.005	10.000	1.475	0.000	0.0140
60 (All)	0.437	1.182	0.004	9.047	1.489	0.032	0.1635
75	0.430	0.370	0.003	5.462	1.759	0.000	0.0267
75 (All)	0.437	1.182	0.004	9.047	1.489	0.032	0.2242
Unpol	0.7	1.7	0.003	3	1.2	0.2	

Table 40. PNT 01006 NIR ss parameters correspond to unpolarized parameters for s and q. The $20°$ case maximizes the q, n, and κ, whereas this does not dominate the 'all' parameters.

θ(deg)	ρ_d	ρ_s	s	q	n	κ	Log. Error
20	0.384	0.063	0.005	10.000	99.963	100.000	0.0239
20 (All)	0.338	0.153	0.002	3.532	1.001	1.430	0.2486
60	0.355	0.103	0.002	3.716	1.004	100.000	0.0306
60 (All)	0.338	0.153	0.002	3.532	1.001	1.430	0.2203
75	0.284	0.107	0.002	3.037	1.000	100.000	0.0331
75 (All)	0.338	0.153	0.002	3.532	1.001	1.430	0.2546
Unpol	0.7	1.7	0.003	3	1.2	0.2	

case, the model does not fit the data well.

Table 41. PNT 01006 NIR polarization term error is lowest for $pp - ss$ in four of six cases compared to $ss - pp$, and $pp - unp$ has better error in three of six cases.

θ	ss-ss	ss-pp	ss-unp	pp-pp	pp-ss	pp-unp
20	0.0239	0.0232	0.0504	0.0189	0.0278	0.0452
20 (All)	0.2486	0.2092	0.2439	0.1958	0.2540	0.2411
60	0.0306	0.1400	0.0936	0.0140	0.0835	0.0978
60 (All)	0.2203	0.2870	0.2770	0.1635	0.2647	0.2995
75	0.0331	0.1877	0.1722	0.0267	0.0444	0.0430
75 (All)	0.2546	0.3903	0.3768	0.2242	0.3345	0.3914
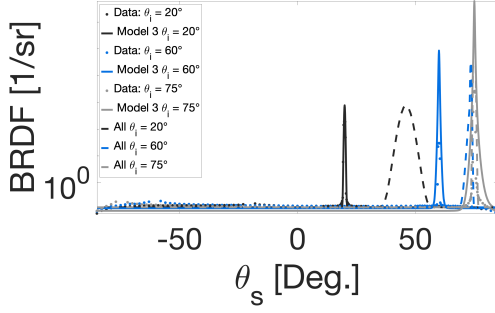
(a) PNT 01006 NIR ss on pp data
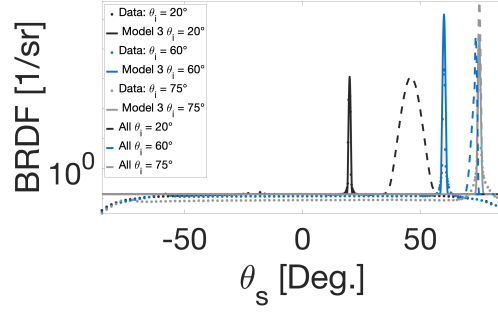
(b) PNT 01006 NIR pp on ss data
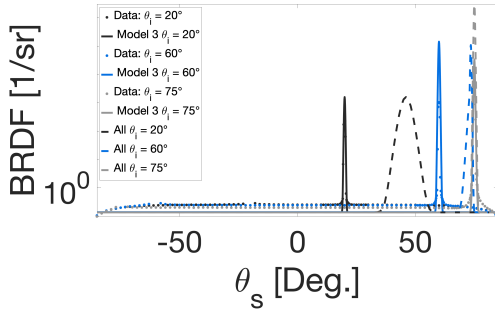
(c) PNT 01006NIR pp on unpolarized data
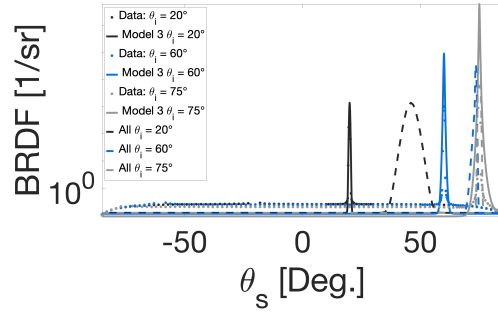
(d) PNT 01006NIR ss on unpolarized data

Figure 28. PNT 01006 NIR has the lowest error for fitting pp parameters on ss polarization in majority crossterm cases

4.9 PNT 01014 NIR

Although it is another glossy material, the fitted parameters for PNT 01014 NIR shown in Tables 43 and 42 and are not similar to those for PNT 1006. The logarithmic error in all cases is higher than that of PNT 01006, but they are comparable between cases. As seen in every other material, the higher incident angle results in a higher error term. All ss polarization cases have n as 1 and the highest incident angle case has a κ of 100. Similarly, one case in the pp polarization case had a κ of 0, which again is not reflective of any realistic material. Also of note is the large value for ρ_s in the highest incident angle pp polarization case. The maximum value allowed for this fitting parameter is 1000, but many of the initial guess parameters had this value at around 935. Similar to the PNT 01006, the pp polarization plot for the middle

incident angle has the lowest BRDF value. In the *ss* polarization case, the BRDF plots do follow a pattern that one would expect in the unpolarized case in Figure 29.
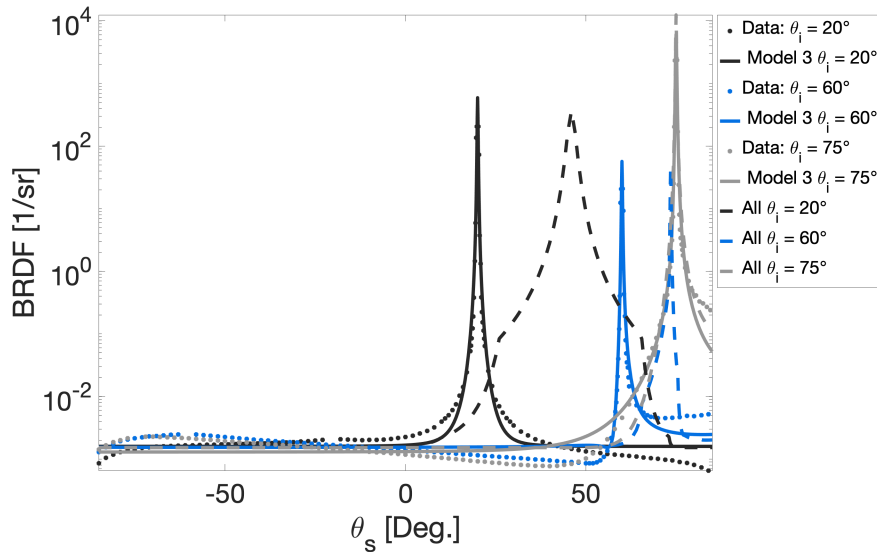
(a) PNT 1014 NIR pp polarization
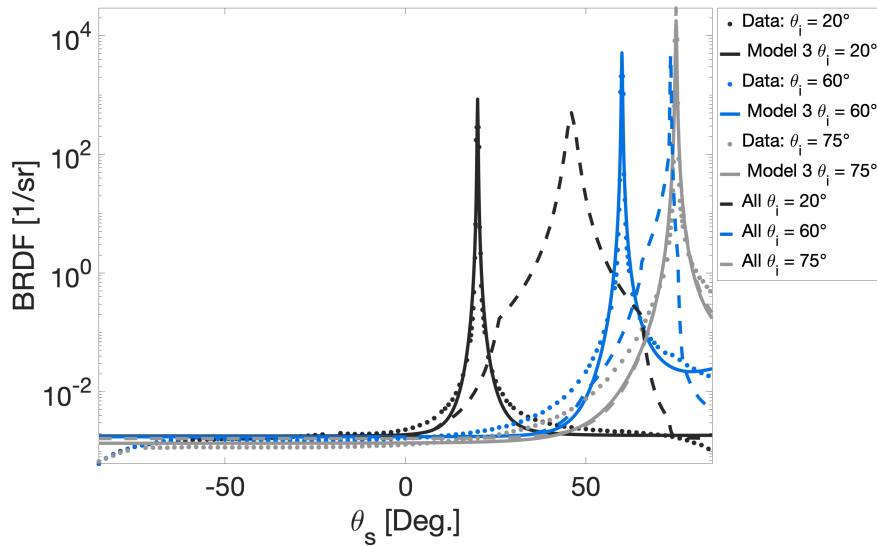
(b) PNT 1014 NIR ss polarization

Figure 29. PNT 1014 NIR data is fitted well when each incident angle has its own optimized parameters. The 'all' parameters modeled with the dashed line do not model the specular peaks at the correct scattered angle.

65

Table 42. PNT 01014 NIR pp parameters are consistent over all cases except for ρ_s at 75° at a value of over 935. Compared to the ss parameters, the n and κ are values other than at the bounds, which may suggest they are more physically realizable.

θ(deg)	ρ_d	ρ_s	s	q	n	κ	Log. Error
20	0.005	2.247	0.001	1.604	1.305	0.004	0.0332
20 (All)	0.005	0.651	0.001	1.500	1.444	0.021	0.4409
60	0.005	2.025	0.001	1.557	1.447	0.000	0.0323
60 (All)	0.005	0.651	0.001	1.500	1.444	0.021	0.2763
75	0.004	935.699	0.001	2.169	1.577	0.003	0.0372
75 (All)	0.005	0.651	0.001	1.500	1.444	0.021	0.4310
Unpol	0.005	1.7	0.003	3	1.2	0.2	

Table 43. PNT 01014 NIR ss parameters are consistent over all cases for ρ_d, s, q, and n. The q and n parameters are both at the minimum bound for almost all cases, which is different than the same parameters in the pp polarization.

θ(deg)	ρ_d	ρ_s	s	q	n	κ	Log. Error
20	0.006	2.395	0.001	1.525	1.000	0.224	0.0332
20 (All)	0.005	0.241	0.001	1.500	1.000	0.738	0.4972
60	0.005	23.297	0.001	1.500	1.000	0.032	0.0374
60 (All)	0.005	0.241	0.001	1.500	1.000	0.738	0.3307
75	0.004	0.121	0.001	1.500	1.000	100.000	0.0434
75 (All)	0.005	0.241	0.001	1.500	1.000	0.738	0.4284
Unpol	0.005	1.7	0.003	3	1.2	0.2	

PNT 01014 cross-term cases in Figures 30(a), 30(b), 30(c), and 30(d) perform similarly to those for PNT 01006. The 20° case shows error that is comparable for all cases, including $ss - ss$ and $pp - pp$ in Table 44. As the incident angle increases, this trend does not hold. The $pp - ss$ and $pp - unp$ cases perform the best for the 60° case. For the 75° case, all cross-term cases are an entire order of magnitude higher than in the lower incident angle cases, with $ss - pp$ performing the worst and $ss - unp$ performing with the lowest error.

(a) PNT 01014 NIR ss on pp data

(b) PNT 01014 NIR pp on ss data

(c) PNT 01014 NIR pp on unpolarized data

(d) PNT 01014 NIR ss on unpolarized data
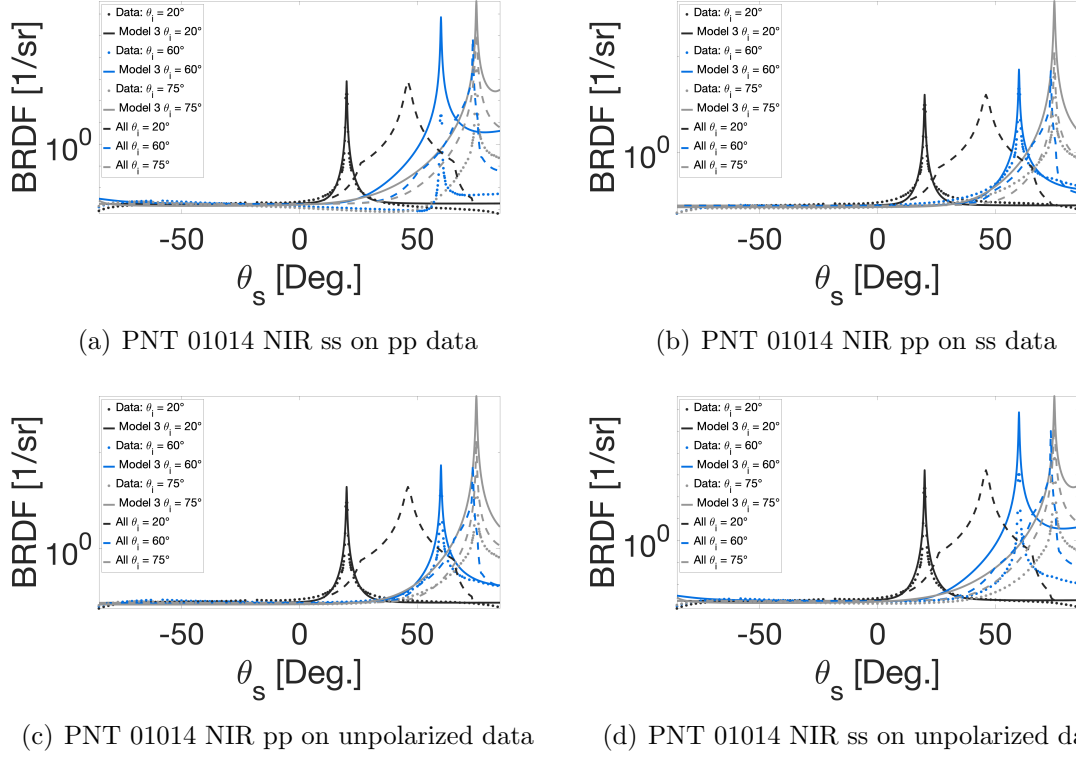
Figure 30. PNT 01014 NIR has a lower error fit for lowest incident angle for ss parameters fitted onto unpolarized data

**Table 44. PNT 01014 NIR polarization term error is lower for four of six cases for both $pp - ss$ and $pp - unp$, but most values are close in value.**

θ	ss-ss	ss-pp	ss-unp	pp-pp	pp-ss	pp-unp
20	0.0332	0.0371	0.0433	0.0332	0.0345	0.0413
20 (All)	0.4972	0.4494	0.4912	0.4409	0.5039	0.4995
60	0.0374	0.3863	0.2480	0.0323	0.0550	0.0759
60 (All)	0.3307	0.4596	0.4133	0.2763	0.3504	0.3642
75	0.0434	0.2921	0.2519	0.0372	0.2605	0.2784
75 (All)	0.4284	0.6428	0.5836	0.4310	0.4775	0.5234

4.10   Parameter Analysis

Comparing the fitted parameters between ss and pp for each material showed that there did not seem to be any correlation. For the same material between different

incident angles, the real part of the index of refraction could range from 1 to nearly 10. This is obviously erroneous as the material properties do not change between different incident angles. The Hyper-Cauchy parameters, s and q were the most effective fitting parameters for how the data is modeled. These also ranged between different incident angles for the same material. In order to compare materials similarly, the parameters were fitted to the material data at 'all' incident angles, meaning all of the data at once. These parameters for both pp and ss polarizations are displayed in Tables 45 and 46.

The most striking difference between the two is the range between the indices of refraction. In the ss polarization case 8 out of the 14 materials had $n = 1.000$ and κ=100.000, suggesting that these terms will require future study in order to determine more realistic parameters. In fact, all but one material, PNT 65 NIR, had n=1, which is not realizable as this is the same as the incident index of refraction, but with different κ. The materials in ss polarization with the highest logarithmic error were the specular materials: PNT 01006, PNT 01014 and the NIST standard materials. Out of these three cases, only one material, PNT 01006 had a q at 1.500. The rest of these materials had q=10, the maximum value, with s ranging from 0.005 to 2.493. Since q is at either its maximum or minimum value in these cases, suspected error within these terms exists as well.

In the pp polarization, erroneous terms exist with the index of refraction terms as well. Out of the 14 materials, 6 materials had an overall $\kappa = 0$ or approximately 0. Only two materials had $n = 1$, but only PNT 65 NIR yielded an index of refraction above 2. Between the two polarization states, no material's index of refraction seems to correlate. As in the ss polarization case, the materials with the highest logarithmic error are the NIST standard materials and the specular paints. All of these cases have κ of approximately 0, and PNT 01006 and PNT 01014 report s of approximately

68

0. For other materials, q is reported at 10 for two materials: PNT 66 NIR and PNT 66 UV, while s ranges between 0 and 10. Overall, the parameters found in the pp polarization seem to have mostly higher logarithmic error values than the ss polarization terms, but since parameter fits in the ss polarization yielded many erroneous index of refraction terms, pp polarization parameters may be technically more reliable.

Table 45. ss parameter comparison for all materials, where 11 of 14 materials report either the maximum or minimum bounds for q, and n

Material	θ(deg)	ρ_d	ρ_s	s	q	n	κ
PNT 65 LWIR	All	0.018	1.450	0.115	1.500	1.000	0.453
PNT 65 MWIR	All	0.028	1.233	0.861	10.000	1.000	0.332
PNT 66 MWIR	All	0.007	1.829	0.319	2.490	1.000	0.428
STD 00696 MWIR	All	0.089	4.287	0.471	2.561	13.781	2.410
STD 00699 MWIR	All	0.073	3.143	0.197	2.449	7.076	0.011
PNT 65 NIR	All	0.353	0.753	0.819	5.644	1.000	0.552
PNT 66 NIR	All	0.012	1.532	0.643	5.327	1.000	0.413
PNT 36375 NIR	All	0.231	5.614	0.207	1.500	1.128	0.000
PNT 01006 NIR	All	0.338	0.153	0.002	3.532	1.001	1.4300
PNT 01014 NIR	All	0.005	0.241	0.001	1.500	1.000	0.738
PNT 65 VIS	All	0.241	5.165	0.750	1.500	1.000	0.409
PNT 36495 VIS	All	0.248	1.087	0.455	3.062	1.000	0.833
PNT 65 UV	All	0.029	2.207	0.585	1.500	1.000	0.556
PNT 66 UV	All	0.015	1.317	0.984	10.000	1.000	0.473

A brief analysis was done using index of refraction parameters for PNT 1006 to fit Fresnel reflectance to the pp parameters to determine indices of refraction. The model was integrated under the specular curve to find unitless reflectance values at different incident and scattered angles. This was done in two ways. First, parameters that were optimized to each individual incident angle were used with the model at each incident angle and at 90°, with the 75° parameters used for 90°. The Fresnel equation, Equation (8) was squared and fitted to the unitless reflectance value from integration. This method, for PNT 1006 calculated $n = 3452.391$ and $\kappa = 3450.503$

69

Table 46. pp Parameter comparison for all materials, where only two of the fourteen materials hit the lower bounds for q and n, compared to the 11 that do in Table 45.

Material	θ(deg)	ρ_d	ρ_s	s	q	n	κ
PNT 65 LWIR	All	0.026	0.888	0.056	1.584	1.354	0.038
PNT 65 MWIR	All	0.017	2.074	0.242	1.570	1.366	0.000
PNT 66 MWIR	All	0.009	2.127	0.302	2.914	1.388	0.030
STD 00696 MWIR	All	0.108	32.243	0.421	3.302	1.679	0.000
STD 00699 MWIR	All	0.098	27.885	0.207	2.967	1.660	0.000
PNT 65 NIR	All	0.353	0.061	4.175	5.450	1.000	4.476
PNT 66 NIR	All	0.011	1.626	0.346	2.884	1.394	0.000
PNT 36375 NIR	All	0.208	0.405	0.962	1.500	1.000	0.022
PNT 01006 NIR	All	0.437	1.182	0.004	9.047	1.489	0.032
PNT 01014 NIR	All	0.005	0.651	0.001	1.500	1.444	0.021
PNT 65 VIS	All	0.227	0.157	5.714	4.074	1.000	4.067
PNT 36495 VIS	All	0.283	0.725	1.179	1.500	1.000	0.069
PNT 65 UV	All	0.021	1.108	0.250	1.500	1.401	0.000
PNT 66 UV	All	0.008	1.989	0.287	2.014	1.411	0.000

with a logarithmic error of 0.000072. A second method used the general parameters for PNT 1006. The model was integrated at every 10 degrees from 0 to 90, and at 75° since PNT 1006 has data at that angle. This method uses 11 points compared to the four points in the first method. Using this method, $n = 3449.983$ and $\kappa = 3448.524$ were determined with a logarithmic error of 0.000026. Both methods found similar values of n and κ, but these are magnitudes larger than values in Table 39. Both methods also had very low logarithmic error, but the number of points is limited in both cases.

4.11   Cross-Term Analysis

Recall in Section 3.1 that $ss - pp$ means ss fit parameters plotted on pp data, and $pp - ss$ means pp fit parameters plotted on ss data. Ideally, the models would produce the same parameters for both ss and pp polarization, as material properties

70

do not vary. These comparisons are performed to quantify how close the results are to this ideal. All materials are represented in Tables 47 and 48 at comparable incident angles for the cases of putting ss fitted parameters on ss and pp polarization data, and vice versa for pp fitted parameters. In all cases, the $ss - ss$ and $pp - pp$ fits have the lowest error, since the respective Rayleigh-Rice term used in the model best fits the data for which the term was meant. As can be seen by the $ss - pp$ and $pp - ss$ columns, which are an order of magnitude higher than the other two columns, using Q_{ss} with pp parameters or Q_{pp} with ss parameters does not produce a comparable fit.

However, between the $ss - pp$ and $pp - ss$ column, the $pp - ss$ column consistently has a lower error. Notably, PNT 65 NIR has similar error values between $ss - pp$ and $pp - ss$. Looking at Figures 10(a) and (b), these fits are plotted and show that in the 30° case, the backscatter is somewhat close, but the rest of the data could not be properly fitted. By far the lowest error term in the cross-term cases is STD 00696 MWIR $pp - ss$ at 0.0088. This is an entire order of magnitude lower than in the $ss - pp$ case at a value of 0.0879. Looking at Figures 24(a) and (b), the ss on pp data case does not closely fit the backscatter data, while the pp on ss plot does.

While the last two materials mentioned differed due to the backscatter data matching the cross-term cases, not all materials behave in that way. For example, PNT 65 UV $pp - ss$ better fits to scattered angles of 0 to 40°. PNT 01006 NIR $ss - pp$ case actually has a lower error than the $pp - ss$ case. This could be due to the material being highly reflective. The only other highly specular material is PNT 01014 NIR, where the cross-term errors are comparable, but the $pp - ss$ case does have a lower error. Compared to the other materials, these errors do not show a preference to diffuse or specular materials. In fact, because the BRDF for specular materials emphasizes the peak over the rest of the data, the parameters are more able to be used

71

interchangeably. Of course, the lowest error even in these materials remains in cases where the Rayleigh-Rice term and the polarization data being fitted are in agreement.

Table 47. The errors calculated in the 60° cross-polarization cases are compared with all of the materials. In 12 of the 14 materials, $pp - ss$ has a lower error than $ss - pp$. For $pp - unp$, 12 of 14 materials have lower error than the $ss - unp$ error.

Material	θ_i (°)	ss-ss	ss-pp	ss-unp	pp-pp	pp-ss	pp-unp
PNT 65 LWIR	60	0.0226	0.2540	0.1849	0.0176	0.1967	0.0824
PNT 65 MWIR	60	0.0092	0.1271	0.0752	0.0098	0.0422	0.0114
PNT 66 MWIR	60	0.0188	0.0812	0.0659	0.0145	0.0307	0.0369
STD 00696 MWIR	60	0.0086	0.2001	0.1974	0.0090	0.0737	0.0838
STD 00699 MWIR	60	0.0103	0.1281	0.1249	0.0107	0.0676	0.0833
PNT 65 NIR	60	0.0006	0.0162	0.0366	0.0020	0.0744	0.0816
PNT 66 NIR	60	0.0025	0.1535	0.0808	0.0041	0.0317	0.0156
PNT 36375 NIR	60	0.0038	0.0930	0.0713	0.0037	0.0139	0.0131
PNT 01006 NIR	60	0.0306	0.1400	0.0936	0.0140	0.0835	0.0978
PNT 01014 NIR	60	0.0374	0.3863	0.2480	0.0323	0.0550	0.0759
PNT 65 VIS	60	0.0036	0.3274	0.1856	0.0021	0.0466	0.0538
PNT 36495 VIS	60	0.0065	0.0915	0.0683	0.0062	0.0480	0.0405
PNT 65 UV	60	0.0054	0.1205	0.0858	0.0148	0.1226	0.0763
PNT 66 UV	60	0.0038	0.1758	0.0915	0.0030	0.0488	0.0372

Comparing over 'all' incident angles for each material, Table 48 also shows that the $pp - ss$ cross-term error is consistently lower than the $ss - pp$ cross-term error. Similarly, the $pp - unp$ error is lower than the $ss - unp$ error, but in the cases that it is not lower, it is very close. In general, fitting to the opposite polarization is more accurate than fitting to the unpolarized data. As seen before, the materials with the highest consistent error across polarization cases are the NIST standard materials and the specular paints.

72

Table 48. Cross-term comparison for all materials, where $pp - ss$ has a lower error than $ss - pp$ for 12 of 14 materials, and $pp - unp$ has a lower error than $ss - unp$ for nine of 14 materials.

Material	θ_i (°)	ss-ss	ss-pp	ss-unp	pp-pp	pp-ss	pp-unp
PNT 65 LWIR	60 (All)	0.1199	0.2222	0.1637	0.1279	0.1208	0.1491
PNT 65 MWIR	60 (All)	0.0772	0.2350	0.1717	0.0999	0.0958	0.1259
PNT 66 MWIR	60 (All)	0.0985	0.2383	0.1623	0.1248	0.1220	0.1323
STD 00696 MWIR	60 (All)	0.1594	0.1228	0.2101	0.1378	0.1300	0.3078
STD 00699 MWIR	60 (All)	0.2800	0.3786	0.3909	0.2303	0.2828	0.4512
PNT 65 NIR	60 (All)	0.0538	0.1405	0.1075	0.0241	0.1183	0.1061
PNT 66 NIR	60 (All)	0.0758	0.3003	0.2086	0.1044	0.1277	0.1299
PNT 36375 NIR	60 (All)	0.0769	0.2192	0.1799	0.0770	0.1059	0.1221
PNT 01006 NIR	60 (All)	0.2203	0.2870	0.2770	0.1635	0.2647	0.2995
PNT 01014 NIR	60 (All)	0.3307	0.4596	0.4133	0.2763	0.3504	0.3642
PNT 65 VIS	60 (All)	0.0298	0.1414	0.0682	0.0267	0.0468	0.0823
PNT 36495 VIS	60 (All)	0.0869	0.1711	0.1309	0.0973	0.0916	0.0962
PNT 65 UV	60 (All)	0.0489	0.1884	0.1423	0.0880	0.0905	0.1258
PNT 66 UV	60 (All)	0.0656	0.1423	0.1265	0.0973	0.1431	0.1300

V. Conclusions and Recommendations

5.1   Conclusions

For an investigation into modeling polarization data using a novel microfacet BRDF model using a Rayleigh-Rice polarization term, fitting parameters were found and modeled on 14 different paints. The accuracy of the Rayleigh-Rice polarization factor had not previously been investigated on polarization data, nor had parameters been found from these data sets before this study. Overall, the parameters are inconsistent between pp or ss polarization. There does not seem to be any correlation between pp or ss parameters, as the parameters vary even for the same material for different incident angles. This is because the model is optimized to best fit the data and gives the fitting parameters for the most optimized case, whether or not they are physically realistic. In fact, most materials had at least one physically problematic term, especially with the indices of refraction.

For investigating whether ss parameters can be used to model pp polarization data, and vice versa, it was found that keeping the parameters with their own respective data resulted in the lowest error. Between using pp parameters on ss polarization data and ss parameters on pp polarization data, pp parameters better modeled ss polarization data than the latter. In the case of modeling unpolarized data, pp parameters better modeled unpolarized data in more cases than ss parameters. In most cases, either ss or pp parameters modeling unpolarized data have lower error than ss parameters on pp polarization data. Consistently, ss parameters on pp polarization data had the highest error. Between diffuse and specular materials, parameters may be more easily interchanged for specular materials since the specular peak dominates the data set compared to diffuse materials which have unique shapes.

In the same way that *pp* parameters modeling *pp* data produces the best results,

the parameters that were from fitting at each incident angle individually had significantly less error than any of the 'all' parameters. While the error is high in these parameters, in the majority of materials, the 'all' parameters were still found to fit the data in each material's respective plots. Backscatter and grazing angle regions were not well fitted by either the separately-optimized-incident-angle parameters or the 'all' parameters. The 'all' parameters for polarization data determined by this model are important to potential remote sensing applications, as a single set of parameters may be used to determine index of refraction, and thus material information. Because it was found that pp parameters are the more accurate set of parameters in general, one would only need the pp polarized parameters to represent a material and determine the index of refraction.

From Table 47, for 12 out of the 14 materials, $pp - ss$ polarization has less error than the $ss - pp$, and $pp - unp$ has less error than $ss - unp$, suggesting that for angles near $60°$, pp polarization data fits data better than ss polarization data. PNT 65 NIR had a higher error in the $pp - unp$ case, but was very close to $ss - unp$. PNT 01006 NIR had higher error in $pp - ss$ than $ss - pp$, but $ss - unp$ had higher error than $pp - unp$. Table 48 also supports this trend. For 12 out of the 14 matierals $pp - ss$ reported lower error than $ss - pp$. For 9 out of 14 materials $pp - unp$ had lower error than $ss - unp$. PNT 01006 NIR, PNT 65 VIS, and PNT 66 UV had lower error in the $ss - unp$ cases, but were fairly comparable to the $pp - unp$ cases. The NIST standard materials had considerably higher error in the $pp - unp$ cases, but this could be due to how the data was fitted in the 'all' case.

In addition to the maximum and minimum bounds for q and n being hit for 11 of 14 materials from Table 45, this indicates that more research must be done on the Q_{ss} term in order to create a more accurate model. Trends indicate that parameters determined from fitting pp polarization data fit cross-polarization terms better than

ss polarization data. Erroneous index of refraction parameters also indicate that more work should be done to increase the accuracy for determining *ss* fitting parameters.

In conclusion, from modeling polarization data, both optimized at each incident angle, and then over 'all' data and performing an error analysis on how the model fits the data, it was found that *pp* parameters best model *ss* and unpolarized data over *ss* parameters. While *ss* parameters modeling *ss* data had a lower error compared to *pp* parameters modeling *ss* data, *pp* parameters modeling *pp* data also had overall lower error. This suggests that the *ss* Rayleigh-Rice term does not perform as well as the *pp* Rayleigh-Rice term. In addition, the upper and lower bounds for the parameters were often hit by *ss* parameters, both in the incident-angle-optimized parameters and the parameters representing 'all' incident angles for a material. The *ss* parameters and fits are unreliable because it shows that for the majority of materials, the *ss* Rayleigh-Rice factor is not properly optimizing all of the parameters, specifically the q and the n. The *pp* Rayleigh-Rice term, shown in Equation (23) does have more terms than the *ss* Rayleigh-Rice term, and this does result in better fits overall. Since the q and n parameters do seem to be the most problematic, looking into the Hyper-Cauchy and *ss* Rayleigh-Rice term would be the best way to improve this novel microfacet model, as that is where the dependence of those parameters is based.

5.2 Recommendations for Future Work

This thesis only considers the accuracy of the Rayleigh-Rice polarization factor and its approximation for the geometric attenuation term in the microfacet BRDF model for these specific materials. Still to be investigated are other BRDF models that account for polarization, the other polarization states, sp and ps, and materials that did not fit well to the model used in this document.

Priest-Germer Microfacet Model.

Another method that should be investigated into the accuracy to account for the polarization of light in terms of BRDF is the Priest-Germer microfacet model. This model approaches the polarization in BRDF models from the viewpoint of using a Jones matrix to describe how an incident electric field is reflected. Note that these are electric field values; to get values for the BRDF, every matrix must be squared. There are four coordinate systems that this model adopts. The first coordinate system gives the reference plane defined by the incident direction and the surface normal, $\hat{\mathbf{z}}$. The second coordinate system is the reference plane defined by the microfacet normal $\hat{\mathbf{n}}$ and incident direction. The third coordinate system is the reference plane defined by the microfacet normal $\hat{\mathbf{n}}$ and the reflected direction. Finally, the fourth coordinate system is the reference plane defined by the reflected direction and surface normal $\hat{\mathbf{z}}$. Mathematically this is shown as [10]

$$\begin{pmatrix} E_s^r \\ E_p^r \end{pmatrix} = \begin{pmatrix} \mathrm{T}_{ss} & \mathrm{T}_{ps} \\ \mathrm{T}_{ps} & \mathrm{T}_{pp} \end{pmatrix} \begin{pmatrix} E_s^i \\ E_p^i \end{pmatrix} \tag{30}$$

where E_s^r and E_p^r are the reflected electric fields, s is perpendicular and p is parallel to the reference frame. This is further broken up into

$$\begin{pmatrix} E_s^r \\ E_p^r \end{pmatrix} = \begin{pmatrix} \cos(\eta_r) & \sin(\eta_r) \\ -\sin(\eta_r) & \cos(\eta_r) \end{pmatrix} \begin{pmatrix} a_{ss} & 0 \\ 0 & a_{pp} \end{pmatrix} \begin{pmatrix} \cos(\eta_i) & -\sin(\mathrm{eta}_i) \\ \sin(\eta_i) & \cos(\eta_i) \end{pmatrix} \begin{pmatrix} E_s^i \\ E_p^i \end{pmatrix} \tag{31}$$

where η_i is the angle that the second coordinate system is rotated away from the first (about the incident direction), η_r is the negative angle that the fourth coordinate system is rotated away from the third (about the reflected direction). a_{ss} and a_{pp} are the Fresnel amplitudes for ss and pp reflection that relate the reflected electric field to the incident electric field. These values are the same as r_p and r_s defined earlier,

77

assuming that the incident light is coming from air, which has an index of refraction of 1.

The polarization component in this model comes in the form of the Jones matrix. Each element of that matrix represents a value for polarization, similar to how the Rayleigh-Rice polarization factor had four different separate equations for each polarization state. This model can give sp and ps polarization fits, but not for data that is in-plane, which is different than the microfacet model.

Cross-polarization terms.

While not considered in this thesis, the polarization cases where light begins in one polarization orientation and is reflected into the other polarization orientation are still vital to most accurately modeling how light physically behaves. In previous work, only unpolarized light was considered, which was calculated using the sum of all the polarization cases [2].

Other materials.

Previous works used up to 18 materials, while this thesis investigates only 14 of those 18 materials [2]. Specifically, STD 00698 was neglected to be investigated in this work because of its lack of sp and ps data. While sp and ps data was neglected in this work because of the low magnitude of the measured BRDF's, it adds more uncertainty to calculate fit parameters to a data set with what seems to be missing data.

In addition, PNT 66 LWIR had uneven sets of data: there was more data for the 60 degree incident angle than the 30 degree incident angle. This occurred because the 60 degree incident angle had smaller scattered angle step sizes than the 30 degree case. While this material does have useful data, it would be erroneous to truncate

www.manaraa.com

data to accommodate how the model in this investigation fits the parameters to the data.

Bibliography

[1] Brian P. Sandford and David C. Robertson. Infrared Reflectance Properties of Aircraft Paints. *Proc. IRIS Targets, Backgrounds, and Discrimination*, 1985.

[2] Becca E. Ewing and Samuel D. Butler. Grazing angle experimental analysis of modification to microfacet BRDF model for improved accuracy. *Proc. SPIE*, 10644, 2018.

[3] Samuel D. Butler, S E. Nauyoks, and M A. Marciniak. Comparison of microfacet BRDF model elements to diffraction BRDF model elements. *Proc. SPIE*, 9472, 2015.

[4] Becca E. Ewing, Samuel D. Butler, and Michael A. Marciniak. Improved grazing angle bidirectional reflectance distribution function model using Rayleigh-Rice polarization factor and adaptive microfacet distribution function. *Optical Engineering*, 57, 2018.

[5] Mark A. Heald and Jerry B. Merion. *Classic Electromagnetic Radiation*. Saunders College Publishing, Orlando, Florida, 1995.

[6] Samuel D. Butler. Experimental and Theoretical Basis for a Closed-Form Spectral BRDF Model. Ph.D. Dissertation, Air Force Institute of Technology, Wright-Patterson AFB, September 2015.

[7] F.E. Nicodemus, J.C. Richmond, J.J. Hsia, I.W. Ginsberg, and T. Limperis. Geometrical considerations and nomenclature for reflectance. *National Bureau of Standards Monograph 160*, Department of Commerce, 1977.

[8] Samuel D. Butler and Michael A. Marciniak. Robust categorization of microfacet BRDF models to enable flexible application-specific BRDF adaptation. *Proceedings of the SPIE*, 9205, 2014.

[9] Szymon M. Rusinkiewicz. A new change of variables for efficient BRDF representation. *Rendering techniques '98*, 1998.

[10] Richard G. Priest and Thomas A. Germer. Polarimetric BRDF in the microfacet model: Theory and measurements. *Proc. 2000 Meeting of the MSS Specialty Sensors Group on Passive Sensors*, 1, 2000.

[11] J.R. Maxwell, J. Beard, S. Weiner, D. Ladd, and S. Ladd. Bidirectional reflectance model validation and utilization. Technical Report AFAL-TR-73-303, Environmental Research Institute of Michigan (ERIM), 1973.

[12] Bui Tuong Phong. Illumination for computer generated pictures. *Communications of the ACM*, 18, 1975.

[13] J.F. Blinn. Models of light reflection for computer synthesized pictures. *Proc. 4th annual conference on computer graphics and interactive techniques*, 1977.

[14] Michael Ashikhmin and Peter Shirley. An anisotrophic Phong BRDF model. *J. Graph Tools*, 5, 2000.

[15] David Wellems, Steve Ortega, David Bowers, Jim Boger, and Matthew Fetrow. Long wave infrared polarimetric model: theory, measurements and parameters. *Journal of Optics A: Pure and Applied Optics*, 8, 2006.

[16] A. Duer. An improved normalization for the ward reflectance model. *J. Graphics, GPU, and Game Tools*, 11, 2006.

[17] K.E. Torrance and E.M. Sparrow. Theory of off-specular reflection from roughened surfaces. *J. Opt. Soc. Am.*, 57, 1967.

REPORT DOCUMENTATION PAGE

1. REPORT DATE *(DD–MM–YYYY)*	2. REPORT TYPE	3. DATES COVERED *(From — To)*
03/26/2020	Master's Thesis	May 2018 — March 2020

4. TITLE AND SUBTITLE

COMPARISON OF THE ACCURACY OF RAYLEIGH-RICE POLARIZATION FACTORS TO IMPROVE MICROFACET BRDF MODELS

5a. CONTRACT NUMBER

5b. GRANT NUMBER

5c. PROGRAM ELEMENT NUMBER

6. AUTHOR(S)

2d Lt Rachel L. Wolfgang

5d. PROJECT NUMBER

5e. TASK NUMBER

5f. WORK UNIT NUMBER

7. PERFORMING ORGANIZATION NAME(S) AND ADDRESS(ES)

Air Force Institute of Technology
Graduate School of Engineering and Management (AFIT/EN)
2950 Hobson Way
WPAFB OH 45433-7765

8. PERFORMING ORGANIZATION REPORT NUMBER

AFIT-ENP-MS-20-M-123

9. SPONSORING / MONITORING AGENCY NAME(S) AND ADDRESS(ES)

Air Force Office of Scientific Research
875 North Randolph St
Ste 325, Room 3112
Arlington, VA 22203

10. SPONSOR/MONITOR'S ACRONYM(S)

AFOSR

11. SPONSOR/MONITOR'S REPORT NUMBER(S)

F4FGA09014J002

12. DISTRIBUTION / AVAILABILITY STATEMENT

APPROVED FOR PUBLIC RELEASE; DISTRIBUTION UNLIMITED.

13. SUPPLEMENTARY NOTES

14. ABSTRACT

Microfacet BRDF models assume that a surface has many small microfacets making up the roughness of the surface. Despite their computational simplicity in applications in remote sensing and scene generation, microfacet models lack the physical accuracy of wave optics models. In a previous work, Butler proposed to replace the Fresnel reflectance term of microfacet models with the Rayleigh-Rice polarization factor, Q, to create a more accurate model. This work examines the novel model that combines microfacet and wave optics terms for its accuracy in the pp and ss polarized cases individually. The model is fitted to the polarized data in each case, using the polarization factor Q, and the resulting fitted parameters are used to investigate whether parameters obtained using the ss and pp polarization may be used on the oppositely polarized or unpolarized data. Parameters fitted from pp polarization data fit cross-term data better than those from ss polarization data for at least nine of the fourteen materials, indicating that more research must be done to make Q in the ss case more accurate. Model trends are determined to guide future work in refining polarimetric models.

15. SUBJECT TERMS

BRDF, polarimetric, optical scatter, microfacet, remote sensing, scene generation

16. SECURITY CLASSIFICATION OF:			17. LIMITATION OF ABSTRACT	18. NUMBER OF PAGES	19a. NAME OF RESPONSIBLE PERSON
a. REPORT	b. ABSTRACT	c. THIS PAGE			Lt Col Samuel D. Butler, AFIT/ENP
U	U	U	U	97	19b. TELEPHONE NUMBER *(include area code)* (937) 255-3636, x4385; samuel.butler@afit.edu